Supervised Reciprocal Filter for OFDM Radar Signal Processing

JAVIER TRUJILLO RODRIGUEZ, Graduate Student Member, IEEE

FABIOLA COLONE, Senior Member, IEEE

PIERFRANCESCO LOMBARDO, Senior Member, IEEE

Sapienza University of Rome, Rome, Italy

In this article, we address the problem of the range-Doppler map evaluation in continuous wave radar exploiting orthogonal frequency division multiplexing (OFDM) signals. This stage is usually implemented by resorting to a suboptimal batches algorithm and a typical choice is to fragment the signal in batches with length equal to the OFDM symbol length and to apply at each batch an appropriate range compression strategy: typically, either matched filter (MF) or reciprocal filter (RF). The former provides the best performance against noise-limited scenarios, whereas the latter against clutter-limited scenarios, thanks to its high peak sidelobe level. Using "OFDM fragmentation" requires symbol synchronization and sets constraints on the coherent processing chain; moreover, we show that it provides a signal-to-noise ratio (SNR) loss both when using MF and RF. Therefore, we investigate the case of "non-OFDM fragmentation," which does not require synchronization and avoids setting constraints on the processing chain. Specifically, we address the case of batch lengths longer than a single OFDM symbol that can potentially reduce the SNR loss at long ranges. We find that this is effective for the MF, but causes an even higher SNR loss for the direct application of the RF filter, which still provides a low level of sidelobes. Aiming at preserving the potential benefits of the RF over the MF against the clutter-limited scenarios, we propose some modified versions of the RF for the non-OFDM fragmentation case, which are shown to offer a tradeoff between SNR losses and sidelobes level control. The effectiveness of the proposed approaches is demonstrated both by providing theoretical performance prediction expressions and by using simulated analyses. To this purpose, a case study is considered for a passive radar exploiting digital video broadcasting – terrestrial transmissions.

Manuscript received 12 May 2022; revised 14 September 2022 and 11 December 2022; accepted 22 December 2022. Date of publication 19 January 2023; date of current version 9 August 2023.

DOI. No. 10.1109/TAES.2023.3235317

Refereeing of this contribution was handled by S. S. Ram.

This work was developed under the support of the Italian Ministero dell.Universit e della Ricerca in the framework of PNRR Partenariati Estesi - Progetto PE14 "RESTART - RESearch and innovation on future Telecommunications systems and networks, to make Italy more smART", CUP B53C22004050001 - D.D. n.1549 del 11/10/2022.

Authors' address: The authors are with the Department of Information Engineering, Electronics, and Telecommunications, Sapienza University of Rome, 00184 Rome, Italy, E-mail: (javier.trujillorodriguez@uniroma1.it; fabiola.colone@uniroma1.it; pierfrancesco.lombardo@uniroma1.it). *(Corresponding author: Javier Trujillo Rodriguez.)*

I. INTRODUCTION

Orthogonal frequency division multiplexing (OFDM) radar uses an OFDM signal as radar waveform. The advantages of OFDM modulation are well established in communication systems, where its use has been consolidated since decades [1]. In contrast, the interest in OFDM technique for radar applications has appeared relatively recently [2]. However, its popularity has increased rapidly being driven by the advancement in hardware capabilities and the growing demand for reciprocal filter (RF) spectral resources.

Specifically, the latter aspect was dealt with from two different perspectives. On one hand, several studies have addressed the possibility to exploit parasitically OFDM transmitters of communication systems as illuminators of opportunity for passive radar (PR) [3], [4], [5], [6], [7], [8], [9], [10], [11], [12], [13]. These included popular state-of-the-art broadcast technologies such as digital video broadcasting – terrestrial (DVB-T) and digital audio broadcasting [3], [6], [8], [9], but also the transmitters for metropolitan and local area networking (e.g., LTE, 5G, Wi-Fi), which are proliferating at rapid rate [10], [11], [12], [13]. This approach makes available a wide set of energy sources that could enable the implementation of PR for the surveillance of wide areas as well as for short range monitoring applications, provided that appropriate signal processing techniques are used to mitigate the effects of the OFDM waveform characteristics, which are not under control of the radar designer.

Another interesting perspective used in OFDM radar research is concerned with the emerging technology of joint radar and communication (JRC) or integrated sensing and communication (ISAC) systems [14], [15], [16], [17]. In fact, the idea of transmitting coded signals via OFDM radar might offer sensible benefits against the increased congestion of the RF spectrum especially in multiuser scenarios such as autonomous driving applications or smart indoor environments. This approach enables the possibility of codesigning the resources shared by the radar and the communication functions, there including the adopted waveform. Still, an important task is to investigate the impact of data transmission on radar performance and to identify methods to facilitate the coexistence.

In both PR and JRC systems, the definition of methods capable of decoupling and relaxing the requirements dictated by the radar and communication functions can make the designer's task easier. This article goes in this direction and addresses the possibility of operating a fundamental radar processing stage beyond the constraints imposed by the framing of an OFDM waveform, typically set to guarantee the desired performance for the communication system.

As is well known, one of the essential signal processing stages in modern radar is the evaluation of the range-Doppler map [18]. When continuous wave transmissions

are used, as for OFDM signals, this is ideally obtained by evaluating the cross-ambiguity function (CAF) between the surveillance signal and a copy of the transmitted signal, namely the reference signal [5]. Apparently, the evaluation of the CAF basically corresponds to the application of a bank of matched filters (MF) tuned to different Doppler frequencies. This approach has two major issues.

First of all, due to the reasonably wide bandwidth of the OFDM signals and the long coherent integration time (CIT) typically considered, the CAF evaluation is computationally expensive. This problem is partially solved by exploiting a fast, suboptimum batching strategy [5], [19]. For OFDM waveforms of opportunity, an obvious choice is to fragment the signal in batches corresponding to individual OFDM symbols. The effect of the Doppler frequency is neglected inside each symbol, which results in inherent losses in terms of signal-to-noise ratio (SNR). However, a large SNR gain is obtained with the final fast Fourier transform (FFT) that is used to integrate the multiple batches available inside the long CIT, thus providing the desired range-Doppler map.

In addition to the limitation abovementioned, we recall that OFDM signals has a number of periodical structures—naming pilot signals, guard interval, or cyclic prefix as examples—needed by the communication function to address problems such as transmitter-receiver synchronization, Doppler-connected distortions, or multipath propagation issues [1]. When exploited for radar purposes, this signal structure results in a CAF characterized by undesired side-peaks and a high sidelobes floor, which might be responsible for ghost targets and severe masking effect on weak target echoes [3], [5], [20].

In the past years, various approaches have been presented in literature to control the sidelobes of the CAF for various types of OFDM-based PR. Among these techniques, the use of a RF has emerged as a widely used approach [6], [7], [21], [22]. This is especially well integrated with the suboptimum CAF, based on batches corresponding to individual OFDM symbols. Specifically, after symbol synchronization, the cyclic prefix is removed from each symbol before moving into the frequency domain, where each subcarrier of the surveillance signal is divided by the corresponding subcarrier of the reference signal. These operations remove both the repetitions in the time domain and the spectral modulation impressed by the transmitted data, providing a perfectly whitened signal, which in turn yields an ideal compression in the time domain. This approach is characterized by additional SNR losses with respect to the use of a MF applied at batch level but provides a low sidelobe response in the range-Doppler domain, which allows it to outperform the MF against clutter-limited scenarios.

The use of the RF in OFDM-based PR and its performance have always been investigated for the case of an OFDM fragmentation, namely when selecting the signal batches to be equal to the OFDM symbols. However, depending on the specific waveform of opportunity and on the extent of the range and Doppler frequency region of interest for the specific surveillance application, the OFDM fragmentation could lead to a performance degradation, due to the constraint on the batch length. Moreover, the possibility to operate using batches whose length is not constrained to be equal to the OFDM symbol provides an increased flexibility to meet some radar requirements such as on the equivalent pulse repetition frequency (PRF), the Doppler ambiguities, and the computational load [5], [19], [23], [24].

Therefore, in this article, we investigate the possibility to operate the RF with batches that do not coincide with individual OFDM symbols, being instead much longer. In principle, this is a more appropriate choice with both the RF and the MF when a wide area surveillance is sought since it allows to limit the SNR losses at long ranges. However, by extending the results in [23], [24], we show that the benefit of a reduced sidelobes level provided by the RF comes with additional non-negligible SNR losses. This is mostly attributed to the need to operate with a signal spectrum that is oversampled with respect to the subcarrier spacing and this in turn results in a noise power boost when using the RF compression strategy.

Consequently, in order to preserve its benefits with respect to the MF against the clutter-limited scenarios, we introduce some modified versions of the RF whose underlying idea is to supervise its application with the aim to make it effective even when operating with an oversampled signal spectrum. Different techniques are proposed by resorting to different strategies to obtain the required control. The need for supervised approaches, as well as the performance improvement that they guarantee, are illustrated in this paper by means of theoretical analyses. Also, their effectiveness is demonstrated when applied against simulated data. To this purpose, the case of a PR is considered based on OFDM transmissions of opportunity. The reported results show that the proposed supervised RF strategies provide a tradeoff between the SNR losses and the sidelobes level. Moreover, they allow to identify the most suitable technique for the application of interest.

The rest of this article is organized as follows. Section II briefly recalls the MF and RF strategies when applied using an OFDM fragmentation and illustrates the inherent limitations. The case of a non-OFDM fragmentation is addressed in Section III, where it is shown that the RF presents high SNR losses. In Section IV, the supervised RF strategies are proposed as a mean to reduce the observed SNR degradation at the cost of higher sidelobes and their performance is theoretically characterized. Moreover, a comparative performance analysis is reported in Section IV where the alternative strategies are applied against a simulated case study. Finally, Section V concludes this article.

II. OFDM SYMBOL BASED RADAR PROCESSING

In modern radar systems, a prior step to target detection is the evaluation of the range-Doppler map [18]. When continuous wave transmissions are used, this is obtained by evaluating the CAF between the surveillance signal $s(t)$, namely the signal collected by the radar antenna, and the reference signal $r(t)$, namely a copy of the transmitted

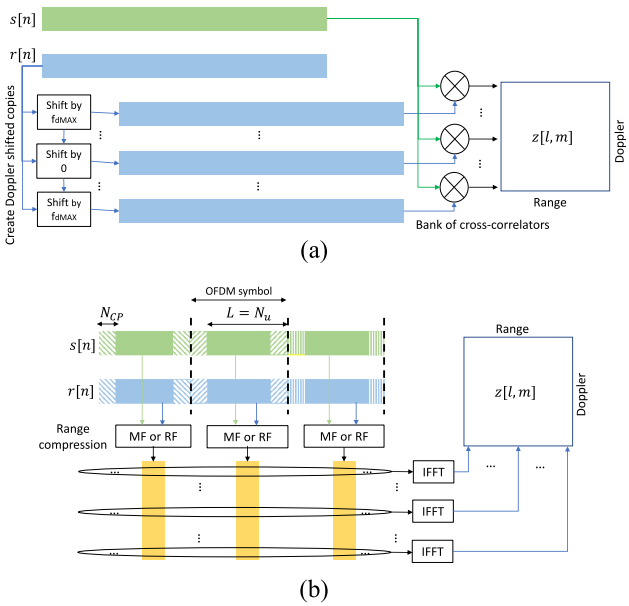

Fig. 1. Processing scheme for the range-Doppler map evaluation by using (a) optimal CAF, (b) suboptimal batches approach with the MF or the RF applied at OFDM symbol level (OFDM fragmentation).

signal. The latter can be assumed to be locally available in JRC (or ISAC) systems; alternatively, it is collected by means of a dedicated receiving channel when PR systems are considered exploiting noncooperative transmitters.

A. Ideal CAF and Batches Algorithm

In discrete time notation, the CAF is evaluated as

$$z\left[l,m\right]=\sum_{n=0}^{N-1}s[n]r^{*}\left[n-l\right]e^{\frac{j2\pi mn}{N}} \tag{1}$$

where $z[l,m]$ is the value of the range-Doppler map at the lth range bin and mth Doppler bin, and N is the number of samples in the CIT of T seconds, assuming a Nyquist sampling of the bandwidth B. Provided that the reference signal is a good copy of the transmitted signal, the evaluation of the CAF basically corresponds to the application of a bank of MFs tuned to different Doppler frequencies, as Fig. 1(a) illustrate.

Whilst it guarantees the best SNR improvement on target echoes, this approach might be computationally intensive, especially when reasonably wide bandwidth signals are used. Therefore, in practical applications, a suboptimum batches algorithm is used instead for the evaluation of the range-Doppler map, which possibly enables a real-time operation while approximating the output of the ideal CAF [5], [19].

When OFDM signals are used, the typical implementation of the suboptimum batches algorithm uses a length of the batches equal to the useful part of the OFDM symbols, after the removal of the cyclic prefix (CP) encompassing N_{CP} samples, which is typically inserted in the signal to remove the effect of multipath and the resulting intersymbol-interference. The effect of the Doppler frequency is neglected inside each symbol, where a zero-Doppler range compression is performed. Then, an IFFT is used to coherently integrate the results from consecutive batches within the CIT. We refer to this approach as the batches algorithm applied with an OFDM fragmentation and has been illustrated on Fig. 1(b). Accordingly, the suboptimal range-Doppler map is obtained as

$$z\left[l,m\right]\cong\frac{1}{L}\sum_{p=0}^{P-1}e^{\frac{j2\pi mp}{P}}\sum_{k=0}^{L-1}S_{p}\left[k\right]H_{p}\left[k\right]e^{\frac{j2\pi kl}{L}} \tag{2}$$

where

1) P is the number of OFDM symbols in the CIT;
2) the inner summation implements the range compression that is performed at FFT speed in the frequency domain $L=N_U$ being the number of non-zero subcarriers in the OFDM symbol;
3) $S_p[k]$ is the discrete Fourier transform (DFT) of the p th OFDM symbol of the surveillance signal, $s_p[n]$, at the kth subcarrier; since an OFDM fragmentation is adopted, $S_p[k]$ takes values drawn from the constellation used by the modulation scheme (e.g., QPSK, 16QAM, and 64QAM).
4) $H_p[k]$ is the range compression filter at the p th batch.

Different choices could be made for the range compression filter according to different objectives. The conventional range compression filter used is the MF that maximizes the SNR at the output of the compression. Alternatively, aiming at the control of the side-peaks and sidelobes floor in the final range-Doppler map, the RF is an attractive mismatched solution [6], [7], [21], [22]. The corresponding filters are specified as

$$H_{p}\left[k\right]=\begin{cases}R_{p}^{*}\left[k\right] & \text{MF}\\ \frac{1}{R_{p}[k]} & \text{RF}\end{cases} \tag{3}$$

where $R_p[k]$ is the reference signal frequency response for the kth subcarrier at the pth OFDM symbol.

B. Performance Metrics

In order to evaluate and compare the performance obtained with the MF and the RF, we need to introduce appropriate performance metrics.

We assume that the surveillance signal only includes the echo from a point-like scatterer located at a particular range bin and Doppler bin $[l_0,m_0]$ corrupted by additive white Gaussian noise. Therefore, we decompose the output map into the sum of the two corresponding contributions: the scatterer echo component $z_S[l,m]$ and the noise component $z_N[l,m]$, namely $z\left[l,m\right]=z_S\left[l,m\right]+z_N[l,m]$.

The output SNR is then defined as

$$\mathrm{SNR}=\frac{\left|E\left\{z_S\left[l_0,m_0\right]\right\}\right|^2}{E\left\{\left|z_N\left[l,m\right]\right|^2\right\}}. \tag{4}$$

Specifically, since this metric is dependent both on the system parameters and on the adopted processing scheme,

in the following we refer to the SNR loss measured with respect to $\mathrm{SNR}_{\max}$, namely the maximum SNR obtained with the ideal CAF in (1), i.e.,

$$\Delta_{\mathrm{SNR}} = \frac{\mathrm{SNR}_{\max}}{\mathrm{SNR}}. \tag{5}$$

The capability to control the sidelobes level in the final map can be measured with reference to two different metrics

1) the peak-to-side-peaks ratio (PSR) metric defined as

$$\mathrm{PSR} = \frac{|E\{z_S[l_0, m_0]\}|^2}{\max\limits_{[l,m]\in I_0} |E\{z_S[l, m]\}|^2} \tag{6}$$

being I_0 the region of interest in the range-Doppler map with the exclusion of an appropriate guard area around the scatterer main peak at $[l_0, m_0]$.
The PSR metric takes into account the sidelobes generated by deterministic components of the OFDM signal (e.g., continuous/scattered pilot signals, cyclic prefix, guard subcarriers) as well as by its average spectral characteristics. The side-peaks encoded in its definition might be responsible of false alarms or local masking effects but are nicely removed when operating with a RF strategy [6], [7], [22]. Also, a quite good control can be obtained if the MF is operated in conjunction with appropriate taper functions provided that the waveform characteristics are known at the receiver [3], [20]. Therefore, despite widely used, the PSR is not the essential performance metric to compare the different approaches to range-Doppler map evaluation, assuming that an appropriate strategy has been used to remove or control the sidelobes due to the deterministic components of the OFDM signal. Therefore, in the following we only consider the following.

2) The sidelobes floor level (SFL) metric defined with respect to the background noise level as

$$\mathrm{SFL} = \frac{var\{z_S[l, m]\}}{E\left\{|z_N[l, m]|^2\right\}}. \tag{7}$$

The SFL metric encodes the effect of the sidelobes level generated by the data-dependent random components of the signals. Its value approximately equals the $\mathrm{SNR}_{\mathrm{in}}$ available at the input of the system (namely before compression) since both the variance of the scatterer echo and the noise contributions increase with the bandwidth-time BT product as per noise-like signals. As for the SNR, in order to quantify the improvement, we refer to the relative SFL with respect to the SFL obtained with the ideal CAF, i.e.,

$$\Delta_{\mathrm{SFL}} = \frac{\mathrm{SFL}}{\mathrm{SFL}_{\mathrm{CAF}}} \tag{8}$$

where $\Delta_{\mathrm{SFL}} < 1$ indicates an improvement, namely a reduction in the random sidelobes level.

Notice that, although not explicitly shown in (8) and (5), both the relative SFL and the SNR loss might be functions of the scatterer location $[l_0, m_0]$ within the map.

Despite the fact that the SFL is defined with reference to a scenario involving a single scatterer echo signal and the noise signal, it can be used as a measure of masking effects caused on weak target echoes when one or more strong target-like echo signals are present in the scenario at different range-Doppler locations. In this case, the desired target peak in the map must compete both against the noise component and against the random sidelobes of the additional strong scatterers that provide their nicely compressed peaks at appropriate range and Doppler bins.

Potential additional target-like echoes include ground clutter echoes from short range, as well as the direct signal interference (that shows as an echo at zero range and Doppler). Typically, both contributions are partially removed by appropriate cancellers in the radar signal processing chain, but, depending on their input power levels, their residuals can still provide a significant random background that affects the desired target peaks in the range-Doppler map. We address the case when this background is higher than the thermal noise component of the CAF as the condition of "clutter-limited" performance, as opposite to the condition of "noise-limited" performance available when this random term is negligible and the only disturbance is provided by thermal noise. Unlike under noise-limited condition, where SNR is the most important metric to determine the detection performance, under clutter-limited condition SFL is the most important parameter to determine the detection capability.

C. MF Versus RF With an OFDM Fragmentation

To operate against clutter-limited scenarios, there is a particular interest for processing schemes providing favorable Δ_{SFL} values. In the previous literature, this motivated the use of the RF filter in place of the MF, providing lower random sidelobes [6], [7], [22]. To show PRO's and CON's of this choice, we discuss the behavior of both the metrics Δ_{SFL} and Δ_{SNR} using a simulated OFDM signal with $N_U =$ 8192 subcarriers and a cyclic prefix equal to $\alpha_{\mathrm{CP}} = N_{\mathrm{CP}}/N_U =$ 1/16 of the useful symbol length, and different modulation constellations (e.g., QPSK, 16QAM, 64QAM). Fig. 2(a) and (b) reports the relative SFL and the SNR loss for a stationary scatterer ($m_0 = 0$) as a function of the scatterer range bin scaled by N_U.

Fig. 2(a) shows that, at ranges corresponding to delays smaller than the CP duration, i.e., $l_0 < N_{CP} = N_U/16$, the MF yields a SFL that depends on the adopted constellation, which basically determines the degree of randomness in the signal power spectrum. Specifically, the relative SFL obtained with the MF applied to OFDM symbols can be predicted by the following formula [22]:

$$\Delta_{\mathrm{SFL}}^{(\mathrm{MF-OFDM})} = \mu - 1 = \frac{1}{M_C} \sum_{q=0}^{M_C-1} \left|c_q\right|^4 - 1 \tag{9}$$

where the constellation dependent coefficient μ is inherently defined, being M_C the constellation size and c_q ($q = 0, \ldots, M_C - 1$) the corresponding symbols. Equation (9) yields $\Delta_{\mathrm{SFL}}^{(\mathrm{MF-OFDM})} = -\infty$ dB for a QPSK, whereas

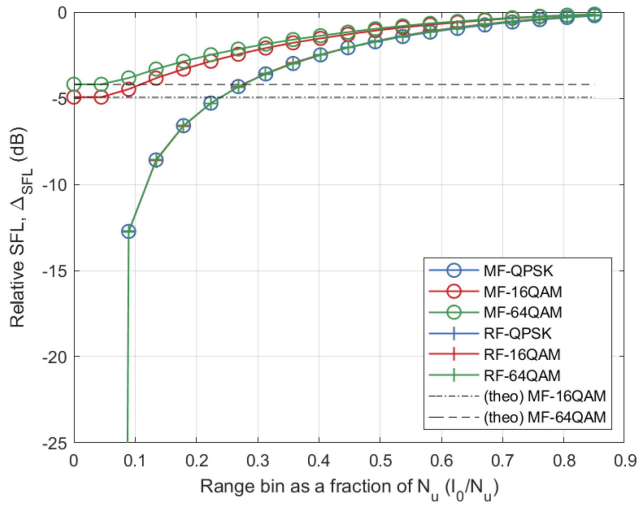

(a)

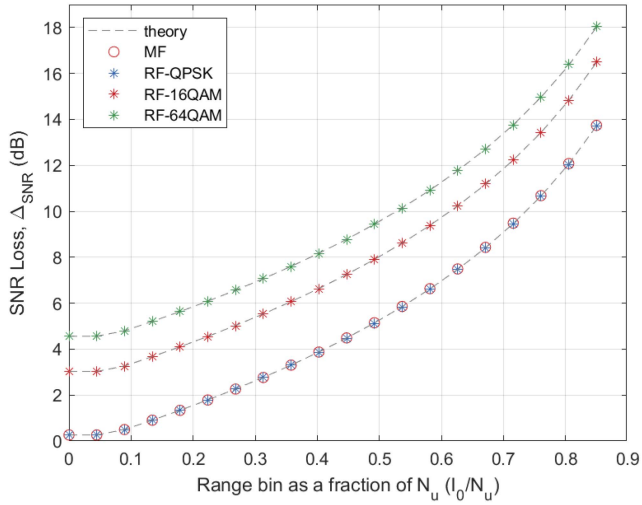

(b)

Fig. 2. Performance comparison of MF and RF range compression strategies applied with an OFDM fragmented signal for a stationary scatterer as a function of the bistatic range. (a) Relative SFL with respect to the ideal CAF. (b) SNR loss with respect to the ideal CAF.

$\Delta_{\text{SFL}}^{(\text{MF}-\text{OFDM})} = -4.95$ dB and $\Delta_{\text{SFL}}^{(\text{MF}-\text{OFDM})} = -4.19$ dB for 16QAM and 64QAM, respectively [see the horizontal dashed curves in Fig. 2(a)].

In contrast, at the same range bins, the RF provides an ideally zero SFL regardless of the employed constellation. This is due to its capability to perfectly equalize the signal spectrum so that the filter response to a point-like scatterer is data independent, namely $z_S[l, m]$ has a deterministic shape with zero variance. Notice that the same effect is present with the MF when a QPSK constellation is adopted, i.e., when using a constellation with equal energy symbols. The conditions above hold up to delays corresponding to the CP extent since the scatterer contribution in each batch coincides with a circularly shifted version of the reference signal. For larger delays, the circular correlation on a symbol basis does not provide perfect focusing for a scatterer echo and the SFL degrades with both the MF and the RF, tending to the SFL of the CAF, namely Δ_{SFL} tends to 0 dB. Specifically, the spectrum equalization provided by the RF is no more perfect for the considered point-like scatterer and the SFL improvement provided by the RF starts decreasing, however it is still better than the MF for a large range extent. This characteristic of the RF has been shown to be largely desirable in order to mitigate the masking effect caused by strong returns from short ranges as well as to enhance the clutter cancellation capability [6], [7], [22]. However, the good SFL control of the RF comes at the cost of a SNR degradation since it is a mismatched filter.

This is shown in Fig. 2(b) that reports the SNR loss to be accepted when the batches algorithm is adopted using an OFDM fragmentation and either a MF- or a RF-based range compression is implemented. For each case, the theoretical SNR loss curves are also reported as dashed lines.

The SNR loss for the batches algorithm that uses the MF with an OFDM fragmentation is reported as a single curve since it does not change with the employed constellation. Nevertheless, it is shown that the loss with respect to the ideal CAF is nonzero and increases with the scatterer range since it reflects the suboptimal operations required by the batches algorithm applied at OFDM symbol level.

To understand the impact of the batch length L on the SNR loss, we provide an analytical formulation. Specifically, it can be expressed as the combination of multiple effects

$$\Delta_{\text{SNR}}^{(\text{MF}-\text{OFDM})} = \rho_{\text{CP}} \cdot \rho_{\text{CC}}\left[l_0, m_0\right] \cdot \rho_{\text{DOP}}\left[m_0\right] \tag{10}$$

where

1) $\rho_{CP} = 1 + N_{CP}/N_U$ is the loss due to the removal of the CP; it is independent of the scatterer location and only depends on the extent of the CP. In our case study, $\rho_{CP} = 0.26$ dB and it corresponds to the loss observed for the MF in Fig. 2(b) at range zero.
2) ρ_{CC} is the loss due to performing the range compression in the frequency domain by taking advantage of the FFT; in fact, the linear correlation is approximated by the circular correlation, which yields an additional SNR degradation at range bins greater than the CP. Specifically, the resulting SNR loss at a particular range-bin l_0 and Doppler-bin m_0 is evaluated as

$$\rho_{CC}\left[l_0, m_0\right] = \begin{cases} 1 & 0 \le l_0 \le N_{\text{CP}} \\ \dfrac{\sin^2\left(\frac{\pi m_0 L}{N}\right)}{\sin^2\left[\frac{\pi m_0 (L - l_0 + N_{CP})}{N}\right]} & l_0 > N_{\text{CP}} \end{cases} \tag{11}$$

where $L = N_U$ for the OFDM fragmentation. Since in Fig. 2(b) we assumed $m_0 = 0$, this term increases as $L^2/(L - l_0 + N_{\text{CP}})^2$ when $l_0 > N_{\text{CP}}$.
2) $\rho_{\text{DOP}}[m_0]$ is the loss caused by the batching strategy that inherently neglects the Doppler-induced phase change within each batch. It can be evaluated as [5]

$$\rho_{\text{DOP}}\left[m_0\right] = \frac{L^2 \sin^2\left(\frac{\pi m_0}{N}\right)}{\sin^2\left(\frac{\pi m_0 L}{N}\right)}. \tag{12}$$

This loss is not visible in Fig. 1(b) since it is evaluated for a stationary scatterer. However, one can easily observe that it increases at larger m_0, i.e., for targets moving at higher bistatic velocities.

The use of the RF in lieu of the MF implies an additional loss $\rho_{\mathrm{RF-OFDM}}$, which is constant across range but depends on the adopted constellation as demonstrated in [22]

$$\Delta_{\mathrm{SNR}}^{(\mathrm{RF-OFDM})} = \rho_{\mathrm{RF-OFDM}} \cdot L_{\mathrm{SNR}}^{(\mathrm{MF-OFDM})} \tag{13}$$

being

$$\rho_{\mathrm{RF-OFDM}} = \zeta = \frac{1}{M_C} \sum_{q=0}^{M_C-1} \left| c_q \right|^{-2}. \tag{14}$$

Such extra loss is zero when a QPSK scheme is used since in that case the RF coincides with the MF, while it is equal to 2.76 dB for a 16QAM and 4.29 dB for a 64QAM. Such values are clearly observed in Fig. 2(b) as a vertical upward shift of the curves obtained for the RF with respect to that of the MF. Based on the good performance in terms of SFL and taking into account the limited entity of this additional loss, we might state that the RF is an attractive solution when the system is not severely limited by the SNR, namely under clutter-limited conditions.

Nevertheless, as is apparent from Fig. 2(b), for both range compression filters, the ρ_{CC} loss becomes unacceptable as the target range increases. Similarly, the ρ_{DOP} loss might become critical at high Doppler frequencies. When operating with an OFDM fragmentation of the signal, such losses are inherently set by the OFDM symbol duration and cannot be adapted to the particular application at hand.

In contrast, from (11), one can observe that ρ_{CC} could be in principle reduced by increasing the batch length L w.r.t. the OFDM symbol duration, namely by resorting to a non-OFDM fragmentation. Similarly, from (12) it is apparent that reducing the batch length could mitigate the ρ_{DOP} loss for high-speed targets. In other words, the reduction of the SNR loss for long range targets could be traded for increased losses for fast moving targets and vice versa.

Therefore, in many applications, it is highly interesting to avoid the constraints of the OFDM fragmentation ($L = N_U$) to exploit a larger flexibility in the selection of the batch length L that could be nicely adapted to meet the coverage requirements either in range or in Doppler. We also observe here that exploiting the batch length flexibly could also make it easier to meet other requirements, e.g., on the equivalent PRF, the Doppler ambiguities, and the computational load.

III. BATCHES ALGORITHM APPLIED WITH NON-OFDM FRAGMENTATION

To overcome the limits of the OFDM fragmentation, we consider an unconstrained batching strategy, where the batch length L can be selected arbitrarily to meet the requirements of the application. We refer to this approach as the batches algorithm applied with a non-OFDM fragmentation.

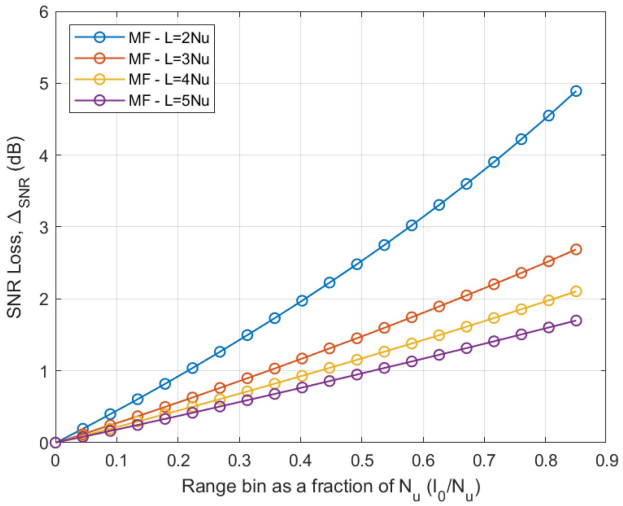

Fig. 3. SNR loss with respect to the ideal CAF for a stationary scatterer as a function of the range bin for MF range compression applied with a non-OFDM fragmented signal using different batch lengths.

Since in a number of practical applications and for several existing OFDM waveforms of opportunity the requirement for a long-range surveillance capability is the most stringent, in this article, we focus on reducing the SNR losses appearing at long ranges by using batches that are longer than the OFDM symbol. In this case, there is no reason to discard the CP, so that all the received signal samples are used for the coherent integration, i.e., $\rho_{\mathrm{CP}} = 0$. Moreover, identifying the OFDM frame start for the surveillance and reference signals is no longer required unless the reference signal has to be demodulated and reconstructed. However, this stage could be avoided when the SNR at the reference channel is high enough; in other words, the collected reference signal can be directly exploited in the processing.

The analysis reported in this section is aimed to understand how the performance of the MF and the RF, both in terms of SNR and SFL, are affected by the batch length selection and how they compare when a non-OFDM fragmentation is adopted.

To assess the effect of the use of long batches, in Fig. 3 we report the relative SNR loss obtained with the MF as a function of the range bin for the same case of Fig. 2(b) and different values of the batch length L. The loss caused by the CP removal is avoided; moreover, the reduction of the loss is apparent, as the batch length increases.

Specifically, the SNR loss yield by the MF can be evaluated as

$$\Delta_{\mathrm{SNR}}^{(\mathrm{MF-non-OFDM})} = \rho_{\mathrm{CC}}\left[l_0, m_0\right] \cdot \rho_{\mathrm{DOP}}\left[m_0\right] \tag{15}$$

where ρ_{CP} is missing thanks to the possibility to retain all the signal samples whereas ρ_{CC} and ρ_{DOP} are given by (11) and (12), respectively, by setting $L > N_u$ and $N_{\mathrm{CP}} = 0$. Compared to the OFDM fragmentation case in Fig. 1(b), the MF applied with a non-OFDM fragmentation clearly provides smaller SNR loss since the constant loss caused by the CP removal is avoided and, more importantly, ρ_{CC}

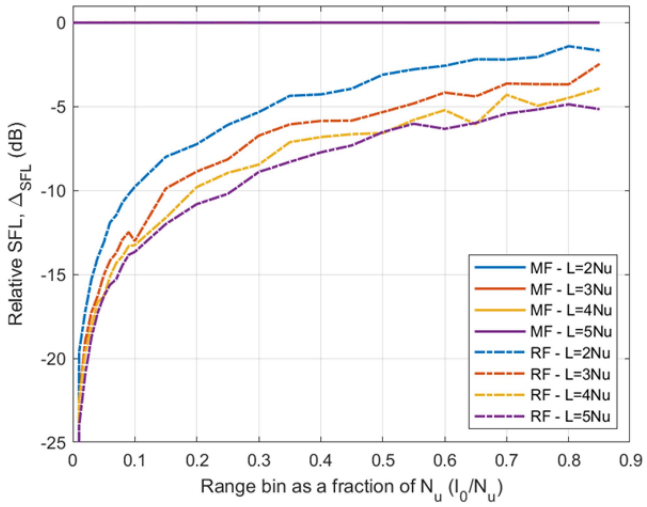

Fig. 4. Relative SFL versus target bistatic range for a stationary scatterer for MF and RF range compression strategies applied with a non-OFDM fragmented signal using different batch lengths.

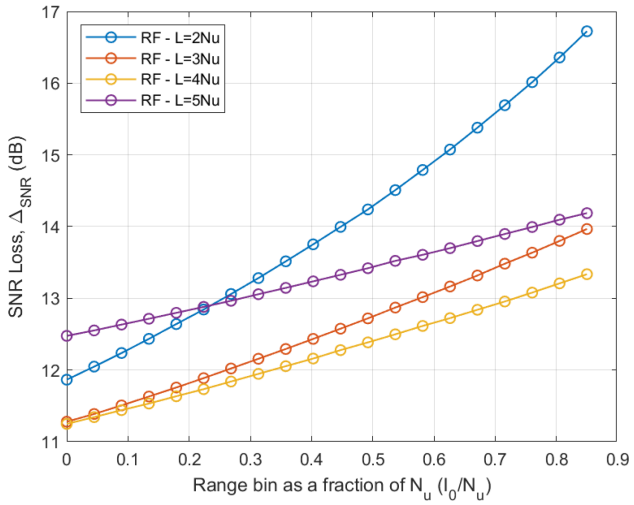

Fig. 5. SNR loss with respect to the ideal CAF for a stationary scatterer as a function of the range bin for RF range compression applied with a non-OFDM fragmented signal using different batch lengths.

reduces as the batch length increases, resulting in SNR loss increasing with smaller slope as a function of the scatterer range bin.

The relative SFL obtained with the MF for the same case of Fig. 1(a) and different values of the batch length L is shown in Fig. 4 (together with the RF) as a function of the range bin.

Unlike the case of an OFDM fragmentation in Fig. 1(a), the SFL obtained with the MF is always coincident with that of the ideal CAF for any value of L. Whilst the curves are reported for a 64QAM constellation, it can be shown that this result does not change with the employed constellation.

Therefore, when operating with longer batches, the MF reduces the SNR losses due to the use of the suboptimum batches algorithm but loses even the little improvement in Δ_{SFL} that it provides when applied with OFDM fragmentation. This confirms its optimality to operate against a noise-limited scenario but does not show a neat improvement of its performance against a strongly clutter-limited scenario.

The behavior of the RF is quite different. We observe that the batch length selection can have a significant impact on the SFL value. The use of OFDM fragmentation provides an optimum SFL thanks to the reduced fluctuation in the signal fragments spectrum. Ideal application of the RF has the potential to make the output map independent of the data content, thus, exactly nulling its variance and hence achieving a zero SFL. When using longer batches, Fig. 4 shows that the RF yields a SFL that is ideally zero only at range zero while it takes nonzero values at nonzero ranges. Consequently, the relative SFL starts decreasing for $l_0 > 0$ rather than after the CP extent, i.e., for $l_0 > N_{CP}$. This is because, for non-OFDM fragmentation, the CP does not help to mitigate the border effect caused by the cyclical correlation within the batch since it does not represent the cyclical extension of the longer batch considered. Consequently, the signal spectrum equalization provided by the RF, which is computed for a zero delay, is not perfect even for targets at short ranges. Therefore, the measured SFL depends on the transmitted signal and fluctuates on different tests and different values of L.

Despite the increase in the first bins, we observe that the RF applied using longer batches still allows a significant improvement in terms of SFL especially for scatterers lying at short ranges. This might still represent a strategic advantage of the RF over the MF against clutter-limited scenarios, since it contributes to mitigate the masking effect caused across the range-Doppler map by strong clutter returns, there including the direct signal from the transmitter, coming from the first range bins. Therefore, the RF filter seems to maintain its appeal for the operation against clutter-limited scenarios.

However, we need to investigate whether the use of longer batches mitigates its high SNR losses especially for long-range targets. Fig. 5 shows the SNR loss for the RF applied against four specific signal realizations using a non-OFDM fragmentation, respectively with $L = 2N_u,\ 3N_u,\ 4N_u$, and $5N_u$.

As for the MF, the slope of the reported curves reduces when the batch length L increases. However, the SNR loss of the RF is characterized by a high (and random) floor, which is generally much larger than for the MF (notice values of $\Delta_{SNR} > 11$ dB even at short ranges). We observe that the high floor has a large variability depending on the specific data samples occurring in the specific simulated signal fragment.

As it is clear, in the case of a non-OFDM fragmentation, the use of the RF in lieu of the MF implies an additional loss that is independent of the adopted constellation but is much higher than that predicted by (14) for the OFDM fragmentation case. Specifically, the SNR loss for the RF

$$\Delta_{\mathrm{SNR}}^{(\mathrm{RF-non-OFDM})} = \rho_{\mathrm{RF-non-OFDM}} \cdot \Delta_{\mathrm{SNR}}^{(\mathrm{MF-non-OFDM})} \quad (16)$$

where $\rho_{\mathrm{RF-non-OFDM}}$ is a data dependent quantity that is likely to take values in the order of several dB.

The abovementioned effect can be qualitatively explained by observing that the use of batches longer than the OFDM symbol duration determines an oversampling in the frequency domain compared to the original sub-carrier spacing. This implies that the DFT of the reference signal does not take only values drawn from the employed constellation but rather its samples spread in amplitude and phase, so that spectral notches are likely to appear. Therefore, when the DFT of the reference signal is inverted to build the RF, these notches produce spikes that, along with the equalization of the signal spectrum, determine a significant amplification of the noise level thus reducing the resulting SNR. The actual loss highly depends on the values and distribution of spectral notches that in turn depend on the data content of the considered signal fragment, and this produces the high variability from batch to batch. Therefore, in order to quantify such effect, the DFT of the reference signal has to be modeled as a random variable.

To this purpose, let us consider the generic bth signal batch and let us assume for simplicity that it includes an integer number Q of OFDM symbols, i.e., $L = Q\ N_S = Q(N_U + N_{CP})$. The reference signal at that batch can be written as

$$\tilde{r}_b(l) = \sum_{q=0}^{Q-1} \sum_{m=0}^{N_U-1} \gamma_{b,p}(m)\, e^{j2\pi \frac{m(l-QN_S)}{N_U}}\, w_{N_S}(l - QN_S) \quad (17)$$

where

- $\gamma_{b,q}(m)$ is the complex symbol transmitted at the mth carrier at the qth OFDM symbol of the bth batch and it takes values out of the employed constellation, i.e., $\gamma_{b,q}(m) \in \{c_r,\ r = 0, \ldots, M_C - 1\}$;
- $w_{N_S}(l)$ is a real-valued time-window that cyclically extends the result of the N_U-points DFT over an interval of duration $N_S = N_U + N_{CP}$. In the following we will assume that a rectangular shaped window is used:

$$w_{N_S}(l) = \begin{cases} \frac{1}{N_S} & 0 < l < N_S - 1 \\ 0 & \text{elsewhere} \end{cases}. \quad (18)$$

The DFT of the signal fragment in (17) is evaluated after straightforward operations as

$$\begin{aligned} \tilde{R}_b(k) &= \sum_{l=0}^{L-1} \tilde{r}_b(l)\, e^{-j2\pi \frac{kl}{L}} \\ &= \sum_{q=0}^{Q-1} \sum_{m=0}^{N_U-1} \gamma_{b,q}(m)\, W_{N_S}\left[\frac{k}{Q} - m\left(1 + \frac{N_{CP}}{N_U}\right)\right] e^{-j2\pi \frac{kq}{Q}} \end{aligned} \quad (19)$$

where $W_{N_S}(k)$ is the DFT of the window $w_{N_S}(l)$ evaluated over N_S samples

$$W_{N_S}(k) = \sum_{n=0}^{N_S-1} w_{N_S}(n)\, e^{-j2\pi \frac{kn}{N_S}}. \quad (20)$$

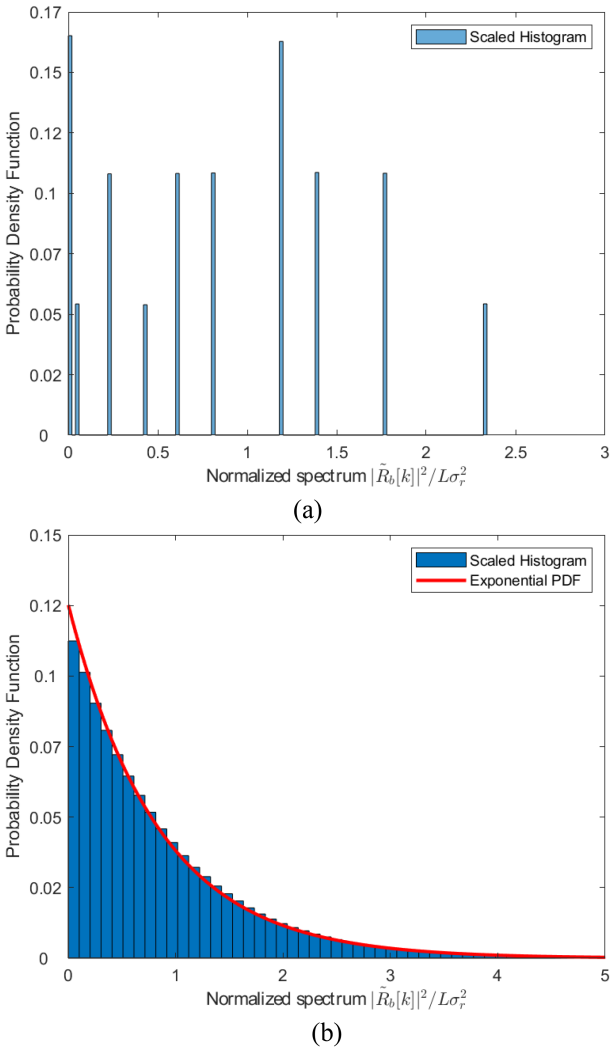

Fig. 6. Probability density function of the reference signal batch power spectrum samples for an OFDM signal when using (a) an OFDM fragmentation $L = N_u$; (b) a non-OFDM fragmentation with $L = 4N_u$.

From (19), taking into account (18), one can easily verify that for $L = N_U$, namely for $Q = 1$ and $N_{CP} = 0$, the DFT of the signal fragment in (17) coincides with the set of symbols transmitted at different subcarriers at that batch encompassing one OFDM symbol. In other words, as expected, when a OFDM fragmentation is adopted, the DFT of the reference signal at each batch takes values drawn from the employed constellation, i.e., $\tilde{R}_b(k) = \gamma_{b,0}(k)$, which can be modeled as discrete random variables. As an example, Fig. 6(a) shows the probability density function (pdf) scaled histogram of the values of $x_b(k) = |\tilde{R}_b(k)|^2$ obtained over multiple batches when using the OFDM fragmentation, i.e., $L = N_u$. As is apparent, the adopted 64QAM constellation results in only nine possible values to be taken with corresponding probability by the spectrum samples amplitude. The zero values correspond to the guard band.

In contrast, when $L > N_U$, the DFT of the reference signal at the bth batch, $\tilde{R}_b(k)$, has samples taken at frequency values that do not coincide with the original subcarriers since the sampling interval is L/N_U smaller than the subcarrier spacing.

Based on (19), it is apparent that each sample does not carry a single symbol drawn from the employed constellation but rather it represents a combination of amplitude scaled and phase distorted symbols transmitted at different subcarriers across consecutive OFDM symbols.

For large N_U and Q, the resulting values can be approximately modeled as complex normal random variables, i.e., $\tilde{R}_b(k) \sim CN(0,\ L\sigma_r^2)$ where σ_r^2 is the reference signal power level. Consequently, by rewriting each sample in terms of its modulus and phase

$$\tilde{R}_b(k) = \sqrt{x_b(k)}\, e^{j\phi_b(k)} k = 0, \ldots, L-1 \qquad (21)$$

we could conclude that $x_b(k)$ is approximately an exponential random variable. As an example, Fig. 6 shows the normalized histogram of the values of $x_b(k)$ obtained over multiple batches when using the non-OFDM fragmentation with a batch length $L = 4N_u$. As apparent, the estimated pdf of the reference signal power spectrum is very close to an exponential pdf.

The range compression filter to be applied at the bth batch can be then redefined as

$$\tilde{H}_b(k) = u_b(k)\, e^{-j\phi_b(k)} k = 0, \ldots, L-1 \qquad (22)$$

where $u_b(k)$ depends on the adopted strategy. For instance

$$u_b(k) = \begin{cases} \sqrt{x_b(k)} & \text{MF} \\ \frac{1}{\sqrt{x_b(k)}} & \text{RF} \end{cases} \quad k = 0, \ldots, L-1. \qquad (23)$$

Accordingly, the additional SNR loss due to the application of a specific range compression strategy can be evaluated as (see Appendix A)

$$\rho = \frac{L\sigma_r^2 E\left\{u_b^2(k)\right\}}{E^2\left\{\sqrt{x_b(k)}u_b(k)\right\}} \qquad (24)$$

that basically represents the SNR loss for a stationary scatterer at zero range. As expected, when a MF is used at each batch, (24) yields a unitary value, namely no additional loss is experienced with respect to those included in (15).

In contrast, for a RF we obtain

$$\rho_{\text{RF}-\text{non}-\text{OFDM}} = L\sigma_r^2 E\left\{\frac{1}{x_b(k)}\right\}. \qquad (25)$$

As apparent, with the abovementioned approximation for the pdf of the power spectrum samples, the additional loss of the RF takes an infinite value. This is because the exponential distribution assigns a nonzero probability to the event of having a zero in the DFT of the reference signal batch. Nevertheless, this result explains the high and variable SNR degradation that the RF suffers when applied using a non-OFDM fragmentation (see Fig. 5).

Both the simulated analysis and the theoretical derivations, confirm that the batches algorithm with a RF applied with a non-OFDM fragmentation using long batches keeps the desirable low SFL characteristic, and therefore, an appeal for the operation against clutter-limited scenarios. However, while the longer batches mitigate the increase of SNR losses at longer ranges, this benefit is spoiled by the appearance of an additional random SNR loss floor, whose statistical motivation has been investigated and understood.

To operate effectively against the clutter-limited scenarios, in the following section, we build upon the statistical analysis above and propose a set of supervised RF filters applicable with the long batches to perform range compression that are able both to preserve the appealing SFL properties of the RF and to limit the global SNR loss.

IV. SUPERVISED STRATEGIES FOR RF IMPLEMENTATION

As the previous section shows, the occurrence of notches in the reference signal batch spectrum is the cause for the RF high SNR degradation when applied with a non-OFDM fragmentation. Hence, to reduce it, we propose different strategies to control the minimum value of the spectral notches before applying the RF. We define these implementations as supervised RF strategies.

Specifically, in all proposed approaches, the range compression filter to be applied at the bth batch is defined as in (22) so that a perfect compensation of the phases across the frequency band is always guaranteed. In contrast, different choices are made for the amplitude of the filter samples $u_b(k)$, thus, obtaining different solutions to the problem at hand. The proposed approaches are illustrated below together with the expected performance (a summary is also reported in Table I).

A. Loaded Reciprocal Filter (LRF)

Since the objective is to control the notches value, a direct approach is to add a constant value x_0 to the reference signal batch power spectrum, which will limit its minimum value. This strategy was preliminary introduced in [23], under the name of LRF, and the corresponding range compression filter is written as

$$u_b(k) = \frac{1}{\sqrt{x_b(k) + x_0}} \quad k = 0, \ldots, L-1. \qquad (26)$$

The constant x_0 should be selected large enough to reduce the SNR loss in (24) while keeping limited the impact on the output spectrum, which should be maintained sufficiently flat in order to preserve the good characteristics of the original RF in terms of relative SFL. To this purpose, based on the exponential model for the variable $x_b(k)$, the SNR loss in (24) is evaluated for the LRF as (see Appendix A)

$$\rho_{\text{LRF}} = \frac{L\sigma_r^2 E\left\{\frac{1}{x_b(k)+x_0}\right\}}{E^2\left\{\sqrt{\frac{x_b(k)}{x_b(k)+x_0}}\right\}} = \frac{e^t E_1(t)}{\frac{\pi}{4}U^2\left(\frac{1}{2}, 0, t\right)} \qquad (27)$$

where $t = x_0/(L\sigma_r^2)$, whereas $E_1(x)$ and $U(a, b, c)$ denote the exponential integral function and the confluent hypergeometric function, respectively.

Similarly, we can write the relative SFL for a scatterer at $l_0 = 0$ for the generic range compression filter as (see

TABLE I
Summary of Range Compression Strategies

Strategy	*Acronym*	*Definition*	Δ_{SNR} *(l=0,m=0)*	Δ_{SFL} *(l=0,m=0)*
Matched Filter	MF	$u_b(k)=\sqrt{x_b(k)}$	1	1
Reciprocal Filter	RF	$u_b(k)=\frac{1}{\sqrt{x_b(k)}}$	∞	0
Loaded Reciprocal Filter	LRF	$u_b(k)=\frac{1}{\sqrt{x_b(k)+x_0}}$	$\frac{e^t E_i(t)}{\left(\frac{\sqrt{\pi}}{2}U(\frac{1}{2},0,t)\right)^2}$	$\frac{1-te^t E_i(t)-\left(\frac{\sqrt{\pi}}{2}U\left(\frac{1}{2},0,t\right)\right)^2}{e^t E_i(t)}$
Thresholded Reciprocal Filter - Saturated	TRF-S	$u_b(k)=\begin{cases}\frac{1}{\sqrt{x_0}} & x_b(k)\le x_0\\ \frac{1}{\sqrt{x_b(k)}} & x_b(k)>x_0\end{cases}$	$\frac{1-e^{-t}+tE_i(t)}{\left(\frac{\sqrt{\pi}}{2}\mathrm{erf}(\sqrt{t})\right)^2}$	$\frac{1-e^{-t}-\left(\frac{\sqrt{\pi}}{2}erf(\sqrt{t})\right)^2}{1-e^{-t}+tE_i(t)}$
Thresholded Reciprocal Filter - Mean	TRF-M	$u_b(k)=\begin{cases}\frac{1}{\sqrt{E\{x_b(k)\}}} & x_b(k)\le x_0\\ \frac{1}{\sqrt{x_b(k)}} & x_b(k)>x_0\end{cases}$	$\frac{1-e^{-t}+E_i(t)}{\left((1-\sqrt{t})e^{-t}+\frac{\sqrt{\pi}}{2}erf(\sqrt{t})\right)^2}$	$\frac{1-te^{-t}-\left((1-\sqrt{t})e^{-t}+\frac{\sqrt{\pi}}{2}erf(\sqrt{t})\right)^2}{1-e^{-t}+E_i(t)}$
Thresholded Reciprocal Filter - Zeros	TRF-Z	$u_b(k)=\begin{cases}0 & x_b(k)\le x_0\\ \frac{1}{\sqrt{x_b(k)}} & x_b(k)>x_0\end{cases}$	$\frac{E_i(t)}{e^{-2t}}$	$\frac{e^{-t}-(e^{-t})^2)}{E_i(t)}$

Appendix B)

$$\Delta_{\mathrm{SFL}}=\frac{E\left\{x_b(k)\,u_b^2(k)\right\}-\left|E\left\{\sqrt{x_b(k)}u_b(k)\right\}\right|^2}{L\sigma_r^2E\left\{u_b^2(k)\right\}} \tag{28}$$

and this can be then specialized for the LRF case as

$$\Delta_{\mathrm{SFL}}^{(\mathrm{LRF})}=\frac{1-te^tE_i(t)-\left(\frac{\sqrt{\pi}}{2}U\left(\frac{1}{2},0,t\right)\right)^2}{e^tE_i(t)}. \tag{29}$$

Incidentally, we observe that (28) yields $\Delta_{\mathrm{SFL}}^{(\mathrm{MF-non-OFDM})}=1$ for the MF and $\Delta_{\mathrm{SFL}}^{(\mathrm{RF-non-OFDM})}=0$ for the RF when applied using a non-OFDM fragmentation of the signal, which is well in line with the results reported in Fig. 4 for $l_0=0$.

B. Thresholded Reciprocal Filter (TRF)

An alternative strategy to supervise the evaluation of the RF is to substitute with a proper constant value α the spectrum samples that fall below a defined threshold. The corresponding range compression filter is written as

$$u_b(k)=\begin{cases}\alpha & x_b(k)\le x_0\\ \frac{1}{\sqrt{x_b(k)}} & x_b(k)>x_0.\end{cases} \tag{30}$$

By making different choices for the value α, a family of supervised strategies is obtained, which is referred to in the following TRF. Specifically, we propose three approaches.

TRF Saturated (TRF-S): In this case, the constant α is selected to match the adopted threshold x_0 so that the spectral samples of the filter are upper-bounded to a desired value, i.e., $\alpha=\frac{1}{\sqrt{x_0}}$.

TRF Mean (TRF-M): An alternative strategy is obtained by selecting the constant α to match the mean spectral power level, i.e., $\alpha=\frac{1}{\sqrt{E\{x_b(k)\}}}=\frac{1}{\sqrt{L\sigma_r^2}}$.

TRF Zeros (TRF-Z): The third approach puts zeros in the filter samples that trigger the threshold, i.e., $\alpha=0$. It is important to remark that this approach was also proposed in [21].

The abovementioned choices determine different performance both in term of capability to recover the SNR loss and in term of relative SFL degradation, and these in turn can be tuned by properly setting the threshold to be used. Table I reports a summary of expected performance for all the four proposed strategies, along with the MF and the RF. Specifically, for each approach, (24) and (28) are evaluated based on the corresponding filter definition and using the statistical model adopted in the previous section (see Appendices A and B for the details).

In addition to the abovementioned strategies, we also consider the.

C. Phase-Only Compensation Filter (PCF)

As an extreme strategy that implements perfect compensation of the phases across the frequency band while exploiting a flat amplitude response so as to avoid any spectral notch. In other words, the filter to be applied at the bth batch is still defined as in (22) with $u_b(k)=1$. We observe that, as the value of the relevant parameter increases, the LRF, the TRF-S, and the TRF-M tend to a PCF and so do their performance. Therefore, the PCF will

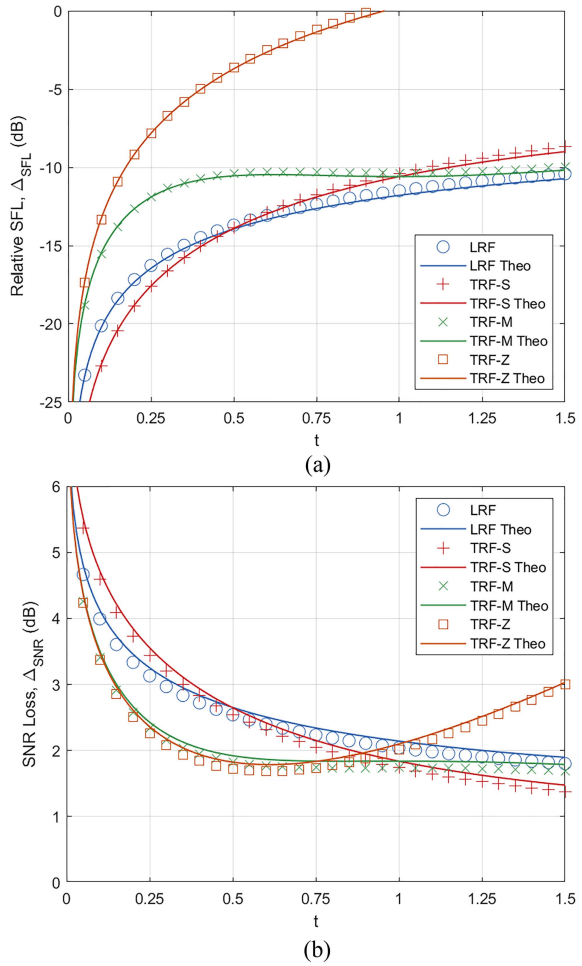

Fig. 7. Performance of the supervised RF strategies as a function of the parameter t for a stationary scatterer at range bin zero, with a non-OFDM fragmentation for $L = 4N_u$: (a) Relative SFL Δ_{SFL}, (b) SNR loss Δ_{SNR}.

be included in the analysis also with the aim to understand the asymptotic performance of the proposed solutions.

The theoretical results of the supervised RF strategies are reported in Fig. 7 as continuous lines for $L = 4N_u$. In addition, markers are used to report the simulated results obtained when the supervised approaches are applied to a generic OFDM signal using a non-OFDM fragmentation with the same batch length L. Specifically, the relative SFL Δ_{SFL} [see Fig. 7(a)] and the SNR loss Δ_{SNR} [see Fig. 7(b)] are shown as a function of $t = x_0/(L\sigma_r^2)$ for a stationary target at range zero. Notice that x_0 is the loading constant in the LRF whereas it represents the adopted threshold in the TRF approaches.

First of all, we observe that there is a substantial agreement between the theoretical and the simulated results. Any difference in each pair of curves is limited to 0.2–0.3 dB. On one hand, this proves the effectiveness of the adopted statistical model approximation for values of the parameter t greater than zero. In fact, with all the approaches, $t > 0$ implies a zero probability to have zeros in the spectrum and this in turn limits the filter samples variance to a finite value. Moreover, the availability of reliable theoretical approximations allows to predict the behavior of different techniques as a function of the relevant parameter and hence to optimize its value. In this regard we observe that, when $t = 0$, no supervision is applied and all the strategies converge to the RF, hence they offer identical performance both in terms of SFL and in term of SNR.

As t increases, the relative SFL degrades with all the proposed strategies [see Fig. 7(a)]. This is an expected result since increasing t corresponds to a heavier modification of the original RF that in turn is data dependent. The degradation is faster for strategies that impose strong discontinuities in the output spectrum, above all the TRF-Z.

Specifically, with this approach the relative SFL takes values above 0 dB when t is greater than 1, meaning that this strategy no longer provides an advantage on the SFL compared to the ideal CAF for those values of t. The LRF and the TRF-S have a comparable behavior since they both imply a moderate modification of the output spectrum for low values of t, thus preserving the advantage of the RF in term of SFL, whereas they tend to spectrally flat range compression filters for large values of t, yielding a limited derivative of the SFL as a function of the parameter. The TRF-M has and intermediate trend since the supervision strategy determines significant spectral transformation at low values of t. However, for larger values of the threshold, a similar effect is observed as for the LRF and the TRF-S since the threshold tends to the mean value of the power spectrum. Actually, it has been verified that these three approaches provide an asymptotic value of the SFL, which corresponds to the that obtained with the PCF $\Delta_{SFL}^{(PCF)} = 1 - \pi/4 \cong -6.1$ dB. It is worth noticing that, with the exception of the TRF-Z, all the supervised strategies provide a SFL lower than the CAF for all the considered values of t. The improvement in term of SFL has to be traded for the expected SNR loss, as shown in Fig. 7(b).

As expected, the SNR loss has an opposite trend as a function of the parameter t. Specifically, as t tends to zero, none of the proposed supervision strategies is effective in removing the spectral notches and the SNR loss tends to that of the original RF. In contrast, as t starts increasing the SNR loss rapidly reduces down to few dB with all the proposed approaches. Interestingly enough, the LRF, the TRF-S, and the TRF-M provide monotonically decreasing loss as the relevant parameter increases so that values below 2 dB are reached for high enough values of t, being the TRF-M the one yielding the faster decay. In this regard, we recall that these filters tend to be spectrally flat as t increases, thus providing an asymptotic value of the SNR loss, which corresponds to the that obtained with the PCF $\rho_{PCF} = 4/\pi \cong 1.04$ dB. In contrast, when using the TRF-Z, the SNR loss reaches a minimum of 1.6 dB at $t \cong 0.6$ but then it starts increasing again. This is due to the fact that, imposing several zeros in the filter amplitude response implies an inherent power loss in the useful signal that is not compensated by the reduction in the output noise.

In order to extend the analysis, Fig. 8 reports the performance of the supervised RF strategies as a function of

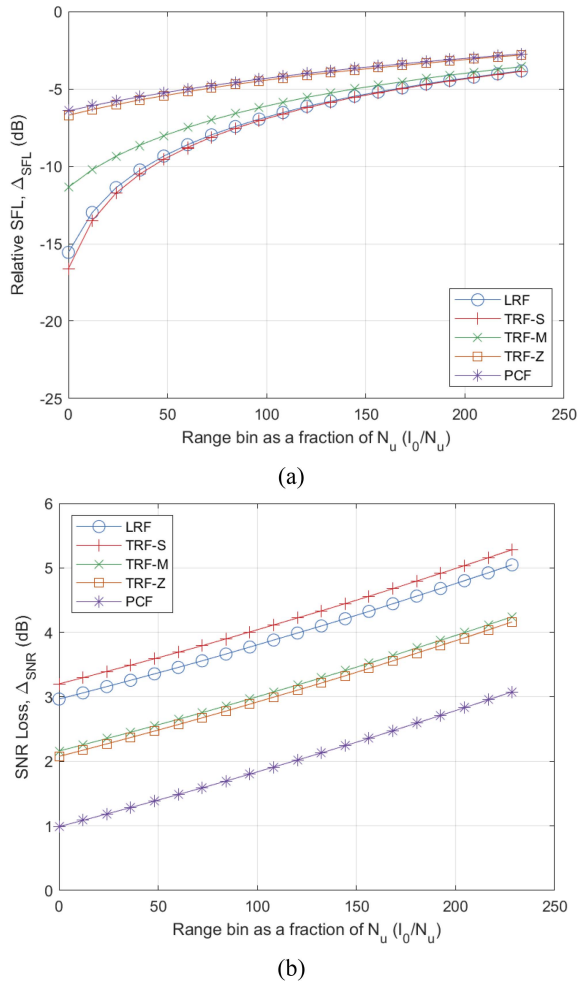

Fig. 8. Performance of the supervised RF strategies for a fixed t as a function of the scatterer range bin, with a non-OFDM fragmentation for $L = 4N_u$: (a) Relative SFL Δ_{SFL}, (b) SNR loss Δ_{SNR}.

the scatterer range bin for a selected value of the relevant parameter, i.e., $t = 0.3$. For a direct comparison, the same case study is considered as in Figs. 2, 3, 4, and 5, and the same scaling strategy is adopted for the abscissa, being the stationary scatterer range bin normalized to the number of useful carriers N_u. All the strategies were applied using a non-OFDM fragmentation of the signal using $L = 4N_u$. Obviously, the performance obtained at range zero are coincident with that observed in Fig. 7 for $t = 0.3$. In this case, also the PCF is reported for comparison.

As is apparent from Fig. 8(b), the SNR loss increases with the scatterer range with the same slope for all the proposed strategies. Moreover, we observe that this slope is the same shown by the RF and MF in Fig. 5 when a batch length of $L = 4N_u$ is considered. This is due to the fact that the SNR loss increase along range is only caused by the loss factors appearing in (15), which only depend on the length of the adopted batch and are not affected by the range compression strategy. Consequently, by reducing the SNR loss at range zero, the supervised strategies are able to limit the SNR loss with respect to the original RF along the whole range extent.

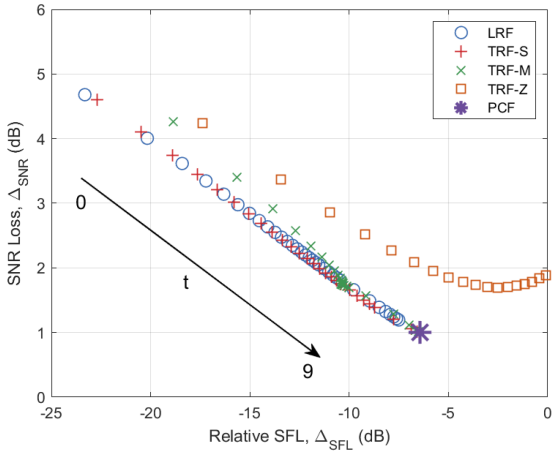

Fig. 9. SNR loss against relative SFL for a stationary scatterer at range zero when using the supervised RF strategies as a function of t.

This advantage is obtained at the price of a relative SFL degradation especially at short ranges. However, all the supervised RF strategies allow to keep a large advantage with respect to the MF. Moreover, there is a tradeoff between the SNR loss and the SFL that can be controlled by the selection of the parameter t, providing a set of flexible solutions that can be adapted to the application requirements.

To further illustrate the tradeoff between the SNR loss and the SFL, Fig. 9 shows Δ_{SNR} against Δ_{SFL} for a stationary scatterer at range zero when the supervised RF strategies are evaluated at values of t between $t = 0$ and $t = 9$. As expected, all the strategies apart from the TRF-Z converge to the PCF performance as t increases. In addition, for a fixed SNR loss, the TRF-Z strategy always has a worst relative SFL than any of the other supervised strategies. This is also true for the TRF-M for low values of t, however, as t increases its performance becomes equivalent to the TRF-S, and the LRF. Finally, we observe that the LRF, and TRF-S offer a similar performance following a line whose derivative approximately trades $\sim$1 dB of SNR loss reduction for $\sim$ 5 dB of increased SFL as t increases.

It is important to highlight that the advantages offered by the proposed range compression strategies are obtained with a negligible increase in terms of computational complexity since the additional operations required by the supervised approach with respect to the RF only involve the evaluation of the modulus of the reference signal spectrum and, in the LRF case, the summation of an additive constant.

Finally, it is worth noticing that the results obtained correspond to a stationary scatterer and they are also valid for low velocity targets. However, the relative sidelobes floor level can be severally degraded for targets moving at high velocities since the presence of high intercarrier interference (ICI) prevents the possibility to perfectly equalize the spectrum and in turn the capability to control the sidelobes level. Nevertheless, the need to control the sidelobes level is crucial for stationary scatterers observed in the first range bins since these are likely to correspond to strong echoes whose sidelobes affect the background level of the entire

TABLE II
Simulation Parameters

Parameter		Value
Coherent integration time (CIT)		0.24 s
Input direct signal-to-noise ratio (DNR_{in})		13 dB
Carrier frequency		600 MHz
Target #1	Input SNR	−20 dB
	Bistatic range	20 km
	Bistatic velocity	5 m/s
Target #2	Input SNR	−40 dB
	Bistatic range	180 km
	Bistatic velocity	10 m/s

range-Doppler maps. In contrast, high Doppler echoes generated by fast moving targets are typically characterized by lower SNR level and rarely responsible of masking effects. Therefore, for those targets, the control of the sidelobes could be unessential since they usually appear below the noise floor.

V. SIMULATION RESULTS

To illustrate the potential advantages of the proposed supervised RF strategies, we consider a simulated case study where a DVB-T based PR is exploited in a maritime surveillance application. In such scenarios, the use of batches longer than the OFDM symbol is advisable since a wide coverage is generally required against targets moving at moderate speeds [25].

The parameters adopted for the simulation are summarized in Table II. We use an 8K DVB-T signal as waveform of opportunity with a 64QAM modulation scheme and all the protocol features such as pilots and cyclic prefix. A CIT of 0.24 s containing $P = 252$ OFDM symbols is exploited. The surveillance signal is generated including direct signal interference and echoes from two targets at different ranges and velocities, with different power levels. The resulting range-velocity maps for different range-compression strategies are reported in Figs. 10 and 11 for the non-OFDM fragmentation case and the OFDM fragmentation case, respectively.

Specifically, Fig. 10(a)–(c) shows the range-velocity maps for the MF, the RF, and one of the proposed supervised RF strategies, respectively, when $L = 4N_u$. Based on the study in Section IV, among the supervised strategies we report the results for the TRF-S operated with a threshold $t = 0.2$ that, as apparent from Fig. 7, offers a relative SFL of about 18 dB while keeping the SNR loss below 4 dB (approximately 3.7 dB). Fig. 11(a) and (b) reports the corresponding results obtained with the MF and the RF applied using batches of length $L = N_u$, hence using the OFDM fragmentation.

In each figure, the position of the two targets has been clearly indicated with white boxes and an enlarged view of the area around the weakest target has been included for visualization purposes. The target peak value represents the output SNR since the map are scaled to the output noise power. The obtained values for the two considered targets are reported in Table III for all the range compression approaches studied in this article (all operating with $t = 0.2$).

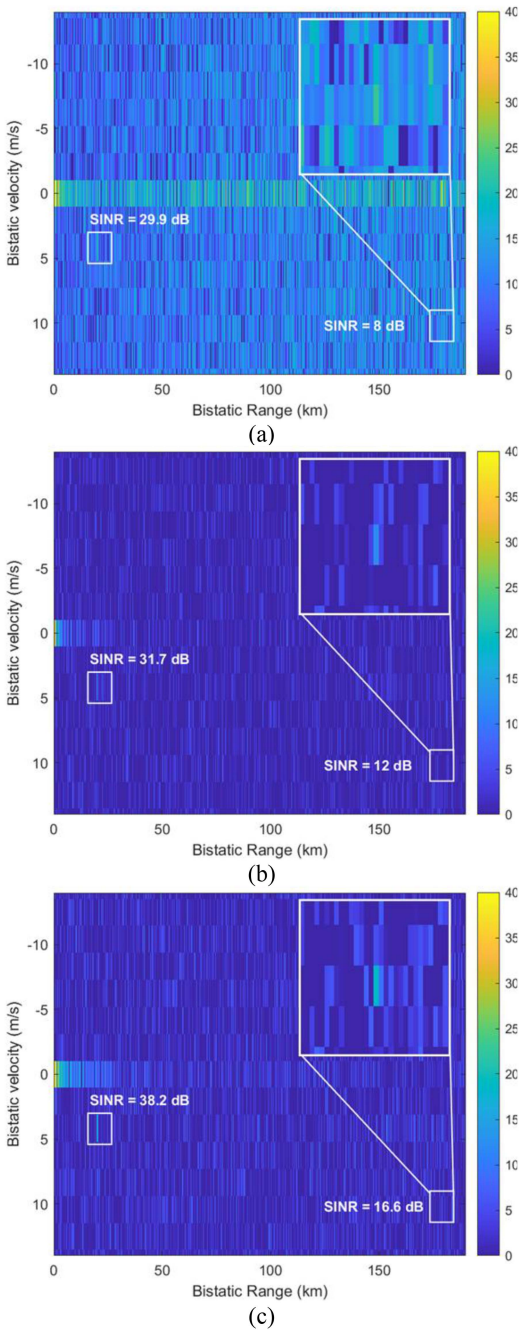

Fig. 10. Range-velocity maps obtained with (a) MF, (b) RF, and (c) TRF-S for a 8K DVB-T signal and a non-OFDM fragmentation with $L = 4N_u$.

As is apparent, the output SNR is reasonably high for target #1 whose echo is generated with a higher input SNR to emulate the case of a target lying at short range (see Table II). In contrast, much lower SNR values are obtained for target #2. In this case, the use of a non-OFDM fragmentation might be very useful to avoid losses due to the circular correlation provided that a MF or a supervised RF strategy is adopted. One may observe that, with all the proposed techniques, the SNR loss mitigation guaranteed by the supervised strategies allows to improve the output SNR value obtained with the MF applied with an OFDM fragmentation. Obviously, they suffer from a SNR loss with respect to the MF applied

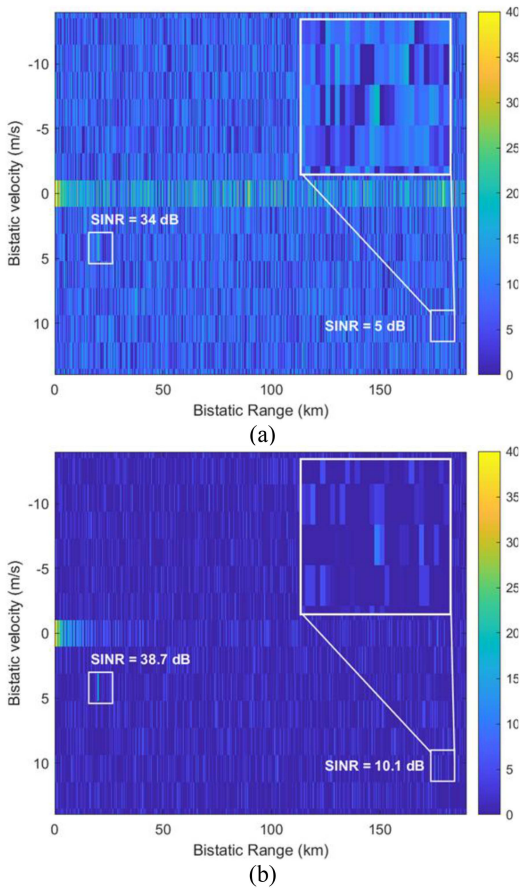

Fig. 11. Range-velocity maps obtained with (a) MF, and (b) RF, for an 8K DVB-T signal and an OFDM fragmentation.

TABLE III
Simulation Results

		Target # 1		Target # 2	
		SNR (dB)	SINR (dB)	SNR (dB)	SINR (dB)
OFDM fragmentation	MF	43.0	34.0	14.0	5.0
	RF	38.7	**38.7**	10.1	10.1
Non-OFDM fragmentation	MF	**43.2**	29.8	**21.3**	8.0
	RF	31.8	31.8	12.0	12.0
	TRF-S	39.4	38.2	17.8	**16.6**
	LRF	39.7	38.2	18.2	16.6
	TRF-M	40.6	37.0	18.9	15.3
	TRF-Z	40.6	34.8	18.8	13.0
	PCF	42.2	34.6	20.4	12.8

using a non-OFDM fragmentation. However, we recall that the motivation behind the use of the RF or its supervised versions is to be found in the need to control the sidelobes floor level possibly caused by disturbance contributions.

This benefit is quite apparent in Figs. 10 and 11, which show a significantly reduced map background level when a RF-based range compression strategy is used. Moreover, this benefit is further investigated in the following by observing that target detection is actually limited by such background level that in turn is determined by the superposition of noise power level P_N and the sidelobes floor power level P_I generated by the strongest interference contributions in the map. In our case study, the latter is due to the sidelobes of the direct signal from the transmitter. To take into account both effects, we evaluate the signal-to-interference plus noise ratio (SINR) as the ratio between the target power P_S and the overall background level against, which it competes

$$\text{SINR} = \frac{P_S}{P_N + P_I} \cong \frac{\text{SNR}}{1 + \text{DNR}_{in} \cdot \Delta_{\text{SFL}}}. \tag{31}$$

In a noise-limited scenario, the background is dominated by the noise level so that the SINR tends to the SNR. In such a case the use of a MF with non-OFDM fragmentation would be the best solution. In contrast, in a clutter-limited scenario, the SINR might be much smaller than the SNR if the range-velocity map is characterized by a high SFL.

The SINR values obtained for the two considered targets are reported in Table III when different approaches are used for range compression. As expected, despite it allows to reach the highest SNR value, the MF operating with a batch length of $L = 4N_u$ yields a generally high SFL so that it shows quite poor SINR values, especially for target #2.

When the RF is applied the best sidelobes reduction is achieved with both fragmentations. This results in a background floor that is dominated by noise, which produces identical values of SNR and SINR. Therefore, when it operates with the OFDM fragmentation, the SINR for both targets is improved with respect to the MF. However, when the RF operates with a non-OFDM fragmentation it suffers from a high SNR loss, which results in a low SINR value at least for target #2.

The selected supervised strategy TRF-S appears to be the best solution for the considered case study. In fact, as it is evident from Fig. 10(c), it achieves a SFL comparable to the RF, which is the result of a good sidelobes reduction. In addition, as predicted by the theory, it suffers from a relatively low SNR degradation compared to the MF operating with $L = 4N_u$. The combined effect results in a high SINR for both targets, especially for the farthest target offering a 4.6 dB increase with respect to the next best solution that in this case is provided by the RF applied with the same batching strategy.

The other supervised RF strategies also offer a remarkable overall SINR compared to the MF and the RF. Specifically, the LRF yields a similar performance than the TRF-S. As expected, the PCF provides the lowest SNR degradation compared to the other supervised strategies but, due to the limited capability to control the sidelobes floor level, it yields the worst SINR among the proposed strategies. Finally, the TRF-M and TRF-Z have a higher SNR than the TRF-S and LRF but a lower SFL reduction, which results in a worse SINR, especially for the TRF-Z. However, it is worth noticing that all the supervised RF strategies provide an improved SINR w.r.t the MF and RF for the farthest target in the considered scenario.

As previously mentioned, the results obtained for the considered case study are highly dependent on the input DNR values. Specifically, high DNR values produce interference-limited scenarios where range compression

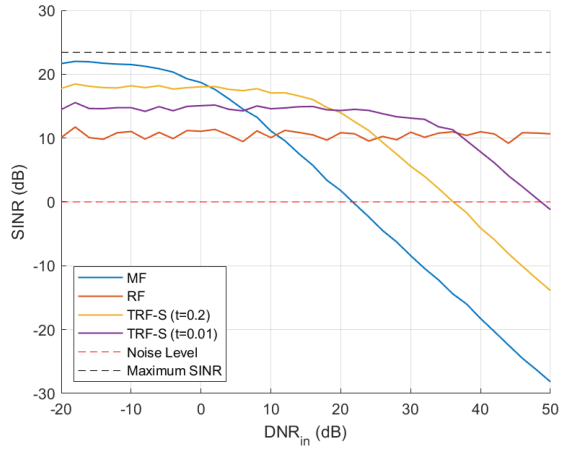

Fig. 12. Target #2 SINR as a function of the input DNR for the MF, RF, TRF-S (t = 0.2), and TRF-S (t = 0.01) operating with a batch length $L = 4N_u$.

strategies with low Δ_{SFL} will perform better. On the other hand, low DNR$_{in}$ values result in noise-limited scenarios where strategies able to preserve the SNR will provide the best performance. To further illustrate this tradeoff we report in Fig. 12 the SINR obtained for target #2 as a function of the input DNR. The results are shown for the MF, the RF, the TRF-S with $t = 0.2$, and the TRF-S with $t = 0.01$ when operating with $L = 4N_u$.

The upper bound to the SINR is reported as a reference in Fig. 12 using a dashed black line and it corresponds to the ideal case of a maximum coherent integration gain with negligible interference. As expected, none of the strategies achieve the maximum SINR because a suboptimum batched strategy is used, which inherently implies some losses.

However, the MF provides the highest SINR for DNR$_{in}$ values below 0 dB as it offers the best SNR. As the DNR$_{in}$ increases, hence, the scenario changes from being noise-limited to being clutter-limited, the MF SINR decreases because of its high sidelobes floor level.

On the other hand, the RF shows a stable, yet low SINR, across the evaluated DNR$_{in}$ range. In particular, it provides the best performance for values of DNR$_{in}$ greater than 36 dB. This is expected, as the RF has the highest sidelobes reduction, which produces a background floor that is dominated by noise for all the DNR$_{in}$ values considered. However, the RF suffers from a high SNR loss when applied with a non-OFDM fragmentation, which results in a poorer performance for low and intermediate DNR$_{in}$ values compared to the MF.

Finally, the TRF-S with both threshold values offer the best SINR for typical values of DNR$_{in}$. This is the result of the combined effect of providing a lower SNR loss than the RF, and a higher sidelobes reduction than the MF. It is important to remark that the performance of the TRF-S is dependent on the selected threshold t. A low value of t will shift the TRF-S towards the RF, having a low SINR overall, but extending the DNR$_{in}$ range where it provides the best performance. This is evident by comparing the performance curves of the TRF-S with $t = 0.01$, and $t = 0.2$. On the contrary, a high value of t will increase the overall SINR at the cost of reducing the DNR$_{in}$ range where it provides the best SINR. This further illustrate the flexibility of the supervised RF strategies and provides a strategy that the designer could use to properly select the parameter t to adapt the solution to the application at hand.

VI. CONCLUSION

In this article, we discussed the limitations of using an OFDM fragmentation for the evaluation of the range-Doppler map based on suboptimal batches algorithm. The need to exploit a non-OFDM fragmentation has been illustrated with batch length longer than the individual OFDM symbol in order to reduce the SNR degradation for targets lying at far ranges. This approach has been proven to be effective when a MF is exploited at the range compression stage whereas a RF-based range compression applied with a non-OFDM fragmentation has been shown to yield additional SNR loss. Therefore, we proposed appropriate supervised strategies as modified versions of the RF that can sensibly reduce the observed SNR loss, while largely preserving the benefits of a RF-based range compression in terms of sidelobes floor level. The performance of the proposed solutions has been theoretically characterized based on a suitable approximation for the signal statistical model. This also provides an effective tool to set the value of their relevant parameters. Moreover, the effectiveness of the proposed approaches has been illustrated by means of simulated analyses using OFDM waveforms. Finally, their benefits have been demonstrated with reference to a practical case study for a DVB-T based PR to be used in maritime surveillance applications.

APPENDIX A
SNR LOSS EVALUATION

In this appendix, the additional SNR loss due to the application of a generic range compression filter is first evaluated and then it is specialized for all the strategies considered in this article.

To this purpose, we start by assuming that the surveillance signal $s[n]$ only includes the echo form stationary scatterer at zero range, i.e., $s[n] = A_s r[n]$, being A_s its complex amplitude. According to (2), the range-Doppler map based on a batches approach applied with a generic fragmentation is given by

$$z_S[l,m] = \frac{A_s}{L}\sum_{b=0}^{B-1} e^{\frac{j2\pi mb}{B}} \sum_{k=0}^{L-1} \tilde{R}_b[k]\,\tilde{H}_b[k]\, e^{\frac{j2\pi kl}{L}} \qquad (32)$$

where $\tilde{R}_p[k]$ and $\tilde{H}_p[k]$ are the FFT of the reference signal and the range compression filter at the bth batch and B is the number of batches. Using (21), (22), (32) becomes

$$z_S[l,m] = \frac{A_s}{L}\sum_{b=0}^{B-1} e^{\frac{j2\pi mb}{B}} \sum_{k=0}^{L-1} \sqrt{x_b(k)}u_b(k)\, e^{\frac{j2\pi kl}{L}}. \qquad (33)$$

Similarly, when assuming that the surveillance signal only includes noise contributions, the output map is

written as

$$z_N[l,m]=\frac{1}{L}\sum_{b=0}^{B-1}e^{\frac{j2\pi mb}{B}}\sum_{k=0}^{L-1}\sqrt{\eta_b(k)}u_b(k)\,e^{j\left[\frac{2\pi kl}{L}-\phi_b(k)\right]} \tag{34}$$

being $\eta_b(k)$ the squared modulus of the FFT of the noise signal at the b-batch.

Therefore, the output SNR is evaluated based on (4) as

$$\mathrm{SNR}=\frac{|A_s|^2\left|\sum_{b=0}^{B-1}\sum_{k=0}^{L-1}E\left\{\sqrt{x_b(k)}u_b(k)\right\}\right|^2}{E\left\{\left|\sum_{b=0}^{B-1}e^{-\frac{j2\pi mb}{B}}\sum_{k=0}^{L-1}\sqrt{\eta_b(k)}u_b(k)e^{j\left[\frac{2\pi kl}{L}-\phi_b(k)\right]}\right|^2\right\}} \tag{35}$$

where the numerator is evaluated at the scatterer location, i.e., $l=l_0=0$ and $m=m_0=0$. Also notice that the expected value at the numerator is evaluated only with respect to the random variable $x_b(k)$ while that in the denominator is evaluated with respect to both the data content and the noise samples. By first evaluating the expected value at the denominator with respect to random noise, we obtain

$$\mathrm{SNR}=\frac{|A_s|^2\left|\sum_{b=0}^{B-1}\sum_{k=0}^{L-1}E\left\{\sqrt{x_b(k)}u_b(k)\right\}\right|^2}{L\sigma_N^2\sum_{b=0}^{B-1}\sum_{k=0}^{L-1}E\left\{u_b^2(k)\right\}} \tag{36}$$

where we assumed that the noise signal is a white process statistically independent of the data content. Moreover, assuming that the statistics of $x_b(k)$ does not change across batches and frequency, (36) can be further simplified as

$$\mathrm{SNR}=\frac{|A_s|^2B\,E^2\left\{\sqrt{x_b(k)}u_b(k)\right\}}{\sigma_N^2\,E\left\{u_b^2(k)\right\}}. \tag{37}$$

Therefore, the SNR loss with respect to the ideal CAF is obtained as [see (5)]

$$\Delta_{\mathrm{SNR}}(l_0=0,\ m_0=0)=\rho=\frac{\frac{|A_s|^2\sigma_r^2BL}{\sigma_N^2}}{\mathrm{SNR}}=\frac{L\sigma_r^2\,E\left\{u_b^2(k)\right\}}{E^2\left\{\sqrt{x_b(k)}u_b(k)\right\}} \tag{38}$$

as reported in (24). We recall that this represents the SNR loss for a stationary scatterer at zero range when a batches approach is applied with a generic signal fragmentation and the range compression filter used at the bth batch is $\tilde{H}_b(k)=u_b(k)e^{-j\phi_b(k)}$.

The abovementioned expression can be specialized to all the cases considered in this article using the exponential approximation for the statistical model of $x_b(k)$ as discussed in Section III. In particular

with the MF, we have $u_b(k)=\sqrt{x_b(k)}$, therefore, we obtain

$$\rho_{\mathrm{MF-non-OFDM}}=\frac{L\sigma_r^2E\{x_b(k)\}}{E^2\{x_b(k)\}}=1 \tag{39}$$

with the RF, we have $u_b(k)=[x_b(k)]^{-\frac{1}{2}}$, and we obtain

$$\rho_{\mathrm{RF-non-OFDM}}=L\sigma_r^2E\left\{\frac{1}{x_b(k)}\right\}=\infty. \tag{40}$$

Similar calculations can be performed for the supervised RF strategies presented in Section IV. Specifically:

for the LRF, using the filter definition in (26), we can write

$$\rho_{\mathrm{LRF}}=\frac{L\sigma_r^2E\left\{\frac{1}{x_b(k)+x_0}\right\}}{E^2\left\{\sqrt{\frac{x_b(k)}{x_b(k)+x_0}}\right\}}. \tag{41}$$

The expected value at the numerator can be obtained as

$$\begin{aligned}E\left\{\frac{1}{x_b(k)+x_0}\right\}&=\int_0^\infty\frac{1}{x+x_0}\frac{1}{L\sigma_r^2}e^{-\frac{x}{L\sigma_r^2}}dx\\&=\frac{e^t}{L\sigma_r^2}\int_t^\infty\frac{1}{z}e^{-z}dz=\frac{e^t}{L\sigma_r^2}E_1(t)\end{aligned} \tag{42}$$

where $t=\frac{x_0}{L\sigma_r^2}$ and $E_1(t)$ is the exponential-integral function.

The expected value at the denominator is derived as

$$\begin{aligned}\sqrt{\frac{x_b(k)}{x_b(k)+x_0}}&=\int_0^\infty\sqrt{\frac{x}{x+x_0}}\frac{e^{-\frac{x}{L\sigma_r^2}}}{L\sigma_r^2}dx\\&=t\int_0^\infty z^{1/2}(1+z)^{-1/2}e^{-tz}dz=\frac{t\sqrt{\pi}}{2}\,U\left(\frac{3}{2},2,\,t\right)\end{aligned} \tag{43}$$

where $U(a,b,t)$ is the confluent hypergeometric function. Using (42) and (43), the SNR loss for the LRF becomes

$$\rho_{\mathrm{LRF}}=\frac{e^tE_1(t)}{\left[\frac{\sqrt{\pi}}{2}U\left(\frac{1}{2},0,t\right)\right]^2} \tag{44}$$

where we have used the Kummer's transformation

$$U(a,b,z)=z^{1-b}U(1+a-b,2-b,z). \tag{45}$$

For a generic TRF, using the filter definition in (30), we can evaluate the expected value at the numerator of (38) as

$$\begin{aligned}E\left\{u_b^2(k)\right\}&=\int_0^{x_0}\alpha^2\frac{1}{L\sigma_r^2}e^{-\frac{x}{L\sigma_r^2}}dx+\int_{x_0}^\infty\frac{1}{x}\frac{1}{L\sigma_r^2}e^{-\frac{x}{L\sigma_r^2}}dx\\&=\alpha^2\left(1-e^{-t}\right)+\frac{1}{L\sigma_r^2}E_1(t).\end{aligned} \tag{46}$$

Similarly, the expected value at the denominator of (38) can be evaluated as

$$\begin{aligned}&E\left\{\sqrt{x_b(k)}u_b(k)\right\}\\&\quad=\int_0^{x_0}\sqrt{x}\alpha\frac{1}{L\sigma_r^2}e^{-\frac{x}{L\sigma_r^2}}dx+\int_{x_0}^\infty\frac{1}{L\sigma_r^2}e^{-\frac{x}{L\sigma_r^2}}dx\\&\quad=\left(1-\alpha\sqrt{L\sigma_r^2}\sqrt{t}\right)\mathrm{e}^{-\mathrm{t}}+\frac{\alpha\sqrt{L\sigma_r^2}\sqrt{\pi}}{2}\mathrm{erf}\left(\sqrt{t}\right).\end{aligned} \tag{47}$$

Consequently, for the TRF-S, being $\alpha=\frac{1}{\sqrt{x_0}}$, the SNR loss becomes

$$\rho_{\mathrm{TRF-S}}=\frac{\frac{1}{t}\left(1-e^{-t}\right)+E_1(t)}{\left[\frac{\sqrt{\pi}}{2\sqrt{t}}\mathrm{erf}\left(\sqrt{t}\right)\right]^2} \tag{48}$$

which coincides with the formula reported in Table I.

Analogously, for the TRF-M, being $\alpha = \frac{1}{\sqrt{E\{x_b(k)\}}} = \frac{1}{\sqrt{L\sigma_r^2}}$, the SNR loss is evaluated as

$$\rho_{\text{TRF-M}} = \frac{1 - e^{-t} + E_1(t)}{\left[\left(1 - \sqrt{t}\right)\mathrm{e}^{-\mathrm{t}} + \frac{\sqrt{\pi}}{2}\mathrm{erf}\left(\sqrt{t}\right)\right]^2} \tag{49}$$

while for the TRF-Z ($\alpha = 0$), we obtain

$$\rho_{\text{TRF-Z}} = \frac{E_1(t)}{\mathrm{e}^{-2\mathrm{t}}}. \tag{50}$$

With the PCF, we have $u_b(k) = 1$, therefore, we obtain

$$\rho_{\text{PCF}} = \frac{4}{\pi}. \tag{51}$$

APPENDIX B
RELATIVE SFL EVALUATION

The SFL is defined in (7) as

$$\text{SFL} = \frac{var\{z_S[l,m]\}}{E\left\{|z_N[l,m]|^2\right\}}. \tag{52}$$

Notice that the denominator coincides with that in (35) so that it can be evaluated as in Appendix A. The variance of the target contribution at the numerator can be decomposed as $var\{z_S[l,m]\} = E\{|z_S[l,m]|^2\} - E^2\{z_S[l,m]\}$. For the expected value, we can easily write

$$\begin{aligned} E\{z_S[l,m]\} &= E\left\{\frac{A_s}{L}\sum_{b=0}^{B-1} e^{\frac{j2\pi mb}{B}} \sum_{k=0}^{L-1} \sqrt{x_b(k)}u_b(k)\, e^{\frac{j2\pi kl}{L}}\right\} \\ &= \begin{cases} A_s B E\left\{\sqrt{x_b(k)}u_b(k)\right\} & l = m = 0 \\ 0 & \text{elsewhere} \end{cases}. \end{aligned} \tag{53}$$

The second moment $E\{|z_S[l,m]|^2\}$ takes the form

$$\begin{aligned} &E\left\{|z_S[l,m]|^2\right\} \\ &= \frac{|A_s|^2}{L^2} E\left\{\left|\sum_{b=0}^{B-1} e^{\frac{j2\pi mb}{B}} \sum_{k=0}^{L-1} \sqrt{x_b(k)}u_b(k)\, e^{\frac{j2\pi kl}{L}}\right|^2\right\} \\ &= \begin{cases} \frac{|A_s|^2 B}{L}\left[\begin{array}{c} E\left\{x_b(k)\,u_b^2(k)\right\} + \\ (BL-1)\,E^2\left\{\sqrt{x_b(k)}u_b(k)\right\} \end{array}\right] \\ m = l = 0 \\ \frac{|A_s|^2 B}{L}\left[\begin{array}{c} E\left\{x_b(k)\,u_b^2(k)\right\} - \\ E^2\left\{\sqrt{x_b(k)}u_b(k)\right\} \end{array}\right] \text{ elsewhere} \end{cases} \end{aligned} \tag{54}$$

where we assumed that data transmitted at consecutive batches is statistically independent.

By using (53) and (54), the numerator of (52) is obtained as

$$\begin{aligned} &var\{z_S[l,m]\} \\ &= \frac{|A_s|^2 B}{L}\left[E\left\{x_b(k)\,u_b^2(k)\right\} - E^2\left\{\sqrt{x_b(k)}u_b(k)\right\}\right]. \end{aligned} \tag{55}$$

Substituting into (52), and using the results for the noise power as in (35), we can write the SFL as

$$\text{SFL} = \frac{|A_s|^2}{L\sigma_N^2}\left[\frac{E\left\{x_b(k)\,u_b^2(k)\right\} - E^2\left\{\sqrt{x_b(k)}u_b(k)\right\}}{E\left\{u_b^2(k)\right\}}\right]. \tag{56}$$

We proceed by evaluating the relative SFL Δ_{SFL} with respect to the ideal CAF using (8)

$$\Delta_{\text{SFL}} = \frac{E\left\{x_b(k)\,u_b^2(k)\right\} - \left(E\left\{\sqrt{x_b(k)}u_b(k)\right\}\right)^2}{L\sigma_r^2 E\left\{u_b^2(k)\right\}}. \tag{57}$$

This result is reported in (28). We recall that this represents the relative SFL for a stationary scatterer at zero range when a batches approach is applied with a generic signal fragmentation and the range compression filter used at the bth batch is $\tilde{H}_b(k) = u_b(k)e^{-j\phi_b(k)}$.

The abovementioned expression can be specialized to all the cases considered in this article using the exponential approximation for the statistical model of $x_b(k)$, as discussed in Section III. Notice that the second term of the numerator and the denominator of (57) were already evaluated in Appendix A. Therefore, we only need to evaluate $E\{x_b(k)u_b^2(k)\}$ for each strategy

with the MF, we have $u_b(k) = \sqrt{x_b(k)}$, therefore, we obtain

$$E\left\{x_b^2(k)\right\} = 2\left(L\sigma_r^2\right)^2 \tag{58}$$

which results in

$$\Delta_{\text{SFL}}^{(\text{MF-no-OFDM})} = \frac{2\left(L\sigma_r^2\right)^2 - \left(L\sigma_r^2\right)^2}{\left(L\sigma_r^2\right)^2} = 1 \tag{59}$$

with the RF, we have $u_b(k) = [x_b(k)]^{-\frac{1}{2}}$, therefore, we obtain

$$E\{1\} = 1 \tag{60}$$

which results in

$$\Delta_{\text{SFL}}^{(\text{RF-no-OFDM})} = \frac{1-1}{L\sigma_r^2 E\left\{\frac{1}{x_b(k)}\right\}} = 0 \tag{61}$$

for the LRF, using the filter definition in (26), we can write

$$\begin{aligned} E\left\{x_b(k)\,u_b^2(k)\right\} &= \int_0^\infty \frac{x}{x+x_0}\frac{e^{-\frac{x}{L\sigma_r^2}}}{L\sigma_r^2}dx \\ &= 1 - x_0\int_0^\infty \frac{1}{x+x_0}\frac{e^{-\frac{x}{L\sigma_r^2}}}{L\sigma_r^2}dx \\ &= 1 - te^t E_1(t) \end{aligned} \tag{62}$$

which result in

$$\Delta_{\text{SFL}}^{(\text{LRF})} = \frac{1 - te^t E_i(t) - \left(\frac{\sqrt{\pi}}{2}U\left(\frac{1}{2},0,t\right)\right)^2}{e^t E_i(t)} \tag{63}$$

for a generic TRF, using the filter definition in (30), we can obtain

$$E\left\{x_b(k)u_b^2(k)\right\} = \int_0^{x_0} \alpha^2 x \frac{e^{-\frac{x}{L\sigma_r^2}}}{L\sigma_r^2}dx + \int_{x_0}^{\infty} \frac{e^{-\frac{x}{L\sigma_r^2}}}{L\sigma_r^2}dx = \alpha^2 L\sigma_r^2 + e^{-t}\left(1-\alpha^2 L\sigma_r^2(1+t)\right). \tag{64}$$

Consequently, for the TRF-S, being $\alpha = \frac{1}{\sqrt{x_0}}$, the SNR loss becomes

$$\Delta_{\text{SFL}}^{(\text{TRF}-\text{S})} = \frac{1-e^{-t}-\left(\frac{\sqrt{\pi}}{2}erf\left(\sqrt{t}\right)\right)^2}{1-e^{-t}+tE_i(t)}. \tag{65}$$

Similarly, for the TRF-M, being $\alpha = \frac{1}{\sqrt{E\{x_b(k)\}}} = \frac{1}{\sqrt{L\sigma_r^2}}$, the relative SFL is evaluated as

$$\Delta_{\text{SFL}}^{(\text{TRF}-\text{M})} = \frac{1-te^{-t}-\left(\left(1-\sqrt{t}\right)e^{-t}+\frac{\sqrt{\pi}}{2}erf\left(\sqrt{t}\right)\right)^2}{1-e^{-t}+E_i(t)} \tag{66}$$

while for the TRF-Z ($\alpha = 0$), we obtain

$$\Delta_{\text{SFL}}^{(\text{TRF}-\text{Z})} = \frac{e^{-t}-\left(e^{-t}\right)^2)}{E_i(t)}. \tag{67}$$

With the PCF, we have $u_b(k) = 1$, therefore, we obtain

$$\Delta_{\text{SFL}}^{(\text{PCF})} = 1 - \frac{\pi}{4}. \tag{68}$$

REFERENCES

[1] R. Prasad, *OFDM for Wireless Communications Systems*. Norwood, MA, USA: Artech House, 2004.

[2] N. Levanon, "Multifrequency radar signals," in *Proc. IEEE Rec. Int. Radar Conf.*, 2000, pp. 683–688.

[3] R. Saini and M. Cherniakov, "DTV signal ambiguity function analysis for radar application," *IEE Proc. Radar Sonar Navigation*, vol. 152, pp. 133–142, Jun. 2005.

[4] C. Berger, B. Demissie, J. Heckenbach, P. Willett, and S. Zhou, "Signal processing for passive radar using OFDM waveforms," *IEEE J. Sel. Topics Signal Process.*, vol. 4, no. 1, pp. 226–238, Feb. 2010.

[5] P. Lombardo and F. Colone, "Advanced processing methods for passive bistatic radar systems," in *Principles of Modern Radar: Advanced Radar Techniques*, W. L. Melvin and J. A. Scheer Eds. Rijeka, Croatia: SciTech, 2012, pp. 739–821.

[6] J. Palmer, H. Harms, S. Searle, and L. Davis, "DVB-T passive radar signal processing," *IEEE Trans. Signal Process.*, vol. 61, no. 8, pp. 2116–2126, Apr. 2013.

[7] G. Gassier, G. Chabriel, J. Barrère, F. Briolle, and C. Jauffret, "A unifying approach for disturbance cancellation and target detection in passive radar using OFDM," *IEEE Trans. Signal Process.*, vol. 64, no. 22, pp. 5959–5971, Nov. 2016.

[8] D. Poullin, "Passive detection using broadcasters (DAB, DVB) with CODFM modulation," *IEE Proc. Radar Sonar Navigation*, vol. 152, pp. 143–152, 2005.

[9] 4. C. J. Coleman and H. Yardley, "Passive bistatic radar based on target illuminations by digital audio broadcasting," *IET Radar Sonar Navigation*, vol. 2, no. 5, pp. 366–375, 2008.

[10] F. Colone, P. Falcone, C. Bongioanni, and P. Lombardo, "WiFi-based passive bistatic radar: Data processing schemes and experimental results," *IEEE Trans. Aerosp. Electron. Syst.*, vol. 48, no. 2, pp. 1061–1079, Apr. 2012.

[11] A. Evers and J. A. Jackson, "Analysis of an LTE waveform for radar applications," in *Proc. IEEE Radar Conf.*, 2014, pp. 200–205.

[12] S. Bartoletti, A. Conti, and M. Z. Win, "Passive radar via LTE signals of opportunity," in *Proc. IEEE Int. Conf. Commun. Workshops*, 2014, pp. 181–185.

[13] P. Samczyński et al., "5G Network-based passive radar," *IEEE Trans. Geosci. Remote Sens.*, vol. 60, 2022, Art. no. 5108209.

[14] B. Paul, A. R. Chiriyath, and D. W. Bliss, "Survey of RF communications and sensing convergence research," *IEEE Access*, vol. 5, pp. 252–270, 2017.

[15] F. Liu, C. Masouros, A. P. Petropulu, H. Griffiths, and L. Hanzo, "Joint radar and communication design: Applications, state-of-the-art, and the road ahead," *IEEE Trans. Commun.*, vol. 68, no. 6, pp. 3834–3862, Jun. 2020.

[16] F. Liu et al., "Integrated sensing and communications: Towards dual-functional wireless networks for 6G and beyond," *IEEE J. Sel. Areas Commun.*, vol. 40, no. 6, pp. 1728–1767, Jun. 2021.

[17] A. Liu et al., "A survey on fundamental limits of integrated sensing and communication," *IEEE Commun. Surv. Tuts.*, vol. 24, no. 2, pp. 994–1034, Apr.–Jun. 2022.

[18] M. A. Richards, J. A. Scheer, and W. A. Holm, *Principles of Modern Radar: Basic Principles*. Raleigh, NC, USA: Shitech Pub., 2010.

[19] C. Moscardini, D. Petri, A. Capria, M. Conti, M. Martorella, and F. Berizzi, "Batches algorithm for passive radar: A theoretical analysis," *IEEE Trans. Aerosp. Electron. Syst.*, vol. 51, no. 2, pp. 1475–1487, Apr. 2015.

[20] F. Colone, D. Langellotti, and P. Lombardo, "DVB-T signal ambiguity function control for passive radars," *IEEE Trans. Aerosp. Electron. Syst.*, vol. 50, no. 1, pp. 329–347, Jan. 2014.

[21] M. Glende, "PCL-signal-processing for sidelobe reduction in case of periodical illuminator signals," in *Proc. Int. Radar Symp.*, 2006, pp. 1–4.

[22] P. Wojaczek, F. Colone, D. Cristallini, and P. Lombardo, "Reciprocal-filter-based STAP for passive radar on moving platforms," *IEEE Trans. Aerosp. Electron. Syst.*, vol. 55, no. 2, pp. 967–988, Apr. 2019.

[23] J. T. Rodriguez, F. Colone, and P. Lombardo, "Loaded reciprocal filter for OFDM-based passive radar signal processing," in *Proc. IEEE Radar Conf.*, 2022, pp. 1–6.

[24] F. Colone, F. Filippini, M. Di Seglio, and K. Chetty, "On the use of reciprocal filter against WiFi packets for passive radar," *IEEE Trans. Aerosp. Electron. Syst.*, vol. 58, no. 4, pp. 2746–2761, Aug. 2022.

[25] T. Martelli, F. Colone, E. Tilli, and A. Di Lallo, "Multi-frequency target detection techniques for DVB-T based passive radar sensors," *Sensors*, vol. 16, no. 10, 2016, Art. no. 1594.

Javier Trujillo Rodriguez (Graduate Student Member, IEEE) received the B.Sc. degree (5.5 years) in telecommunications engineering from Instituto Balseiro, San Carlos de Bariloche, Argentina, in 2018. He is currently working toward the Ph.D. degree in radar and remote sensing with the Department of Information Engineering, Electronics, and Telecommunications, Sapienza University of Rome, Rome, Italy.

From February 2019 to November 2019, he was a Data Scientist for Telefonica Argentina. He was involved in research projects funded by the Italian Government. His main research interests include adaptive signal processing for OFDM-based and passive bistatic radar systems.

Fabiola Colone (Senior Member, IEEE) received the Laurea degree (B.S.+M.S.) in telecommunications engineering and the Ph.D. degree in remote sensing from Sapienza University of Rome, Rome, Italy, in 2002 and 2006, respectively.

She was with the Department of Information Engineering, Electronics, and Telecommunications, Sapienza University of Rome as a Research Associate in January 2006. From December 2006 to June 2007, she was a Visiting Scientist with the Department of Electronic and Electrical Engineering, University College London, London, U.K. She is currently a Full Professor with the Faculty of Information Engineering, Informatics, and Statistics, Sapienza University of Rome. The majority of his research activity is devoted to radar systems and signal processing. She has been involved, with scientific responsibility roles, in research projects funded by the European Commission, the European Defence Agency, the Italian Space Agency, the Italian Ministry of Research, and many radar/ICT companies. Her research has been reported in more than 160 publications in international technical journals, book chapters, and conference proceedings. He is coeditor of the book *Radar Countermeasures for Unmanned Aerial Vehicles* (IET Publisher, London, U.K.).

Dr. Colone has been corecipient of the 2018 Premium Award for Best Paper in IET Radar, Sonar and Navigation. Since 2017, she has been member of the Board of Governors of the IEEE Aerospace and Electronic System Society (AESS) in which she was a Vice-President for Member Services, and Editor-in-Chief for the IEEE Aerospace and Electronic Systems Society (AESS) QEB Newsletters. She is a member of the IEEE AESS Radar System Panel from 2019. She is an Associate Editor-in-Chief for IEEE TRANSACTIONS ON RADAR SYSTEMS. She was Associate Editor for IEEE TRANSACTIONS ON SIGNAL PROCESSING and is member of the Editorial Board of the *International Journal of Electronics and Communications* (Elsevier, New York, NY, USA). She was with the organizing committee and in the technical program committee of many international conferences. She was Technical co-Chair of the IEEE 2021 Radar Conference (Atlanta, USA) and of the European Radar Conference EuRAD 2022 (Milan, Italy).

Pierfrancesco Lombardo (Senior Member, IEEE) received the Graduate degree in electronic engineering and the Ph.D. degree in remote sensing from the University of Rome "La Sapienza," Rome, Italy, in 1991 and 1995, respectively.

After serving with the Official Test Centre of the Italian Air Force in 1992, he was an Associate with Birmingham University, U.K., and with Defence Research Agency in Malvern, in 1994. In 1995, he was a Research Associate with Syracuse University, Syracuse, NY, USA. In 1996, he was with the University of Rome "La Sapienza," where he is currently a Full Professor. He is involved in, and coordinates, research projects funded by European and National Research Agencies and national industries. He leads the "Radar, Remote Sensing, and Navigation" group, University of Rome "La Sapienza." He chairs the Cosmo-SkyMed consulting group for the Italian Space Agency. His research has been reported in more than 280 publications in international technical journals and conferences and five book chapters. His main research interests include radar adaptive signal processing, radar clutter modeling, radar coherent detection, passive radar and multistatic radar, SAR processing, and radio-localization systems.

Dr. Lombardo was a corecipient of the Barry Carlton Award (Best Paper) of IEEE TRANSACTIONS ON AEROSPACE AND ELECTRONIC SYSTEMS in 2001 and of the Best Paper Award for IEEE TRANSACTION ON GEOSCIENCE AND REMOTE SENSING in 2003. He was the technical committee of many international conferences on radar systems and signal processing. He was a Technical Committee Chairman of the IEEE/ISPRS Workshop on Remote Sensing and Data Fusion over Urban Areas URBAN'2001, Rome, URBAN'2003, Berlin, and URBAN'2005, Tempe, USA, and also a Technical Chairman of the IEEE Radar Conference 2008. He is an Associate Editor for Radar Systems for IEEE TRANSACTIONS ON AEROSPACE AND ELECTRONIC SYSTEMS (AES) since June 2001, and a Technical Editor for Radar System since January 2016. He is a member of the IEEE AES RADAR SYSTEM PANEL and the Editorial Board of *IET Proceedings on Radar, Sonar, and Navigation*.